Construction of New Infrared Reflection Absorption Spectroscopy (IRRAS) System for Solid-Solution Interface Biomaterials

Md. Abu Sayed

Doctor of Philosophy

Department of Structural Molecular Science
School of Physical Science
The Graduate University of Advanced Studies

2009

To

My parents

&

Supervisors

(Prof. T. Urisu, SOKENDAI, Japan,
Prof. M. Huque, BUET, Bangladesh &
Prof. C. M. Mustafa, RU, Bangladesh)

Abstract

The study of protein–surface interactions represents one of the most important topics in the field of biomaterials. The immobilization of proteins on solid surfaces is an important step in biosensor fabrication as well as medical devices. Infrared spectroscopy is a powerful technique for the determination of conformation and orientation of lipids and proteins including membrane proteins, and of antibody-antigen reactions on solid surfaces. Infrared reflection absorption spectroscopy (IRRAS) is one of the FT-IR techniques for determination of biomaterials on IR reflective metals, and very few IRRAS systems are found to determine the adsorbate at solid-solution interfaces.

For my doctoral research work, I have constructed a new narrow gap infrared reflection absorption spectroscopy (NG-IRRAS) system with a prism/narrow solution layer/substrate arrangement, to which substrates for biosensors and biochips can be directly attached. Advantages of this new NG-IRRAS system over other conventional-IR systems are i) different IR reflective materials can be used as a substrate ii) having a sufficient large gap (~8 μm) to flow reagent solution, and iii) a solution injection system is included to introduce reagent solution onto the sample substrate from outside. Another advantage of this IRRAS system is that this system can easily be rearranged to vacuum IRRAS system. There were two problems to be solved for the standardization of this NG-IRRAS system, i) the baseline was fluctuated due to the change of solution layer thickness, and ii) sample biomaterials was adsorbed on prism surface.

In the first stage of my PhD work, I constructed the new NG-IRRAS system and investigated the conditions for the flat and stable baseline. Firstly, it was found that baseline was fluctuated due to the change of solution layer thickness. I developed a new sample holder for controlling the solution layer thickness between the prism and substrate surfaces (Fig. 1). Thermal effects, adsorbed water on the entrance of optical components, bubbles in solution, and injection flow rate were considered as factors which distorted the baseline. I have investigated the experimental conditions and found that the following procedures are crucial for the stability of the baseline: i) evacuation of the sample chamber at least for 6 h was necessary to minimize the adsorbed water vapor effect, ii) injection flow rate was kept less then 2 mL/h, iii) room temperature fluctuation was controlled within 1°C, and iv) Ni spacer thickness was 8 μm.

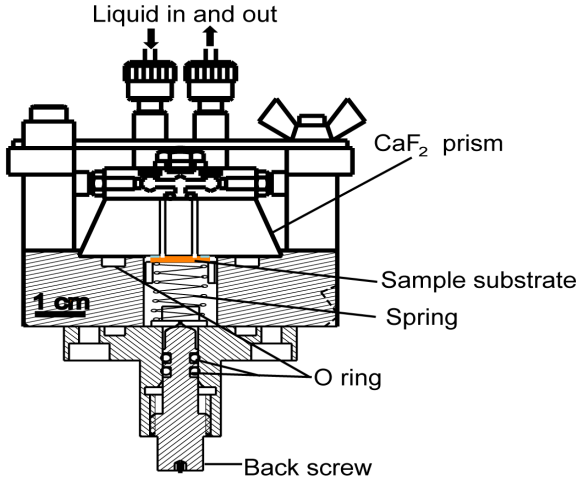

Fig. 1 Schematic diagram of the sample holder for solid-solution interface IRRAS measurement.

After the standardization of the NG-IRRAS, I started the IRRAS measurement of solid surfaces in three different conditions. i) The observation of CaF_2 prism surface in total internal reflection (TIR) mode to investigate the adsorbed biomaterials on prism surface. ii) The observation of biomaterials

adsorbed at the interface between the sample substrate and solutions. Two IR-reflective substrates, Si wafer with buried metal layer (BML) and gold were used. iii) The observation of adsorbed biomaterials on the solid surface in vacuum.

Fibronectin (FN) and immunoglobulin G (IgG) were selected for observation at solid-solution interface. But, during the experiments, IR absorbance from the adsorbed biomaterials on the prism surface overlapped the IRRAS spectra of the biomaterials on the sample substrate. Thus, I controlled the adsorption of biomaterials on the prism surface by regulating the effects of salt and pH of the solution and by coating the CaF_2 prism with 2-methoxy-(polyethylene) oxypropyltrimethoxysilane (PEG). Interestingly, the adsorption tendency on the prism surface was completely opposite with salt effects between these two biomaterials (Fig. 2).

FN is easily adsorbed on SiO_2 surface and often used as an extra cellular matrix in the cell culture on SiO_2 substrates. Therefore, FN was chosen in this work to detect at BML-solution interface. I have investigated the condition, in which FN adsorbed only on the BML surface, but not on the PEG-coated prism surface. I found that FN adsorbed on the prism surface in D_2O based phosphate buffered saline (PBS) solution, but ignorable adsorbed FN was found on the PEG-coated prism surface when pure D_2O was used in the experiment (Fig. 2a).

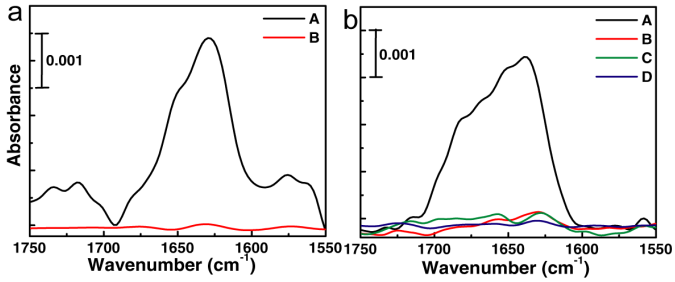

Fig. 2 The amide I bands of adsorbed proteins on a PEG-coated prism surface measured with the total internal reflection (TIR) arrangement.
a) Spectra of FN using (A) D_2O-based PBS solution and (B) pure D_2O as solvents,
b) Spectra of IgG using (A) pure D_2O, (B) NaCl (140 mM) D_2O solution, (C) D_2O-based PBS solution and (D) NaCl-added (140 mM) D_2O-based PBS solution as solvents.

The IRRAS of adsorbed FN was observed at BML-D_2O interface using this condition. The protein amide I band appear in the range of 1600 – 1700 cm^{-1} assigned to the C=O stretching. The fine structure in the amide I supplies the information of the protein secondary structure, because the peak shift of υ (C=O) due to the hydrogen bonding characteristics of the secondary structure, e.g. υ (C=O) of β-sheet at 1613 -1638 cm^{-1}, α-helix at 1645 - 1657 cm^{-1} , and β-turn at 1662 -1683 cm^{-1}. The amide I band of FN was observed at approximately 1637 cm^{-1} (β sheet) with shoulders around 1671 and 1683 cm^{-1} (β turn) (Fig. 3a). The ignorable conformational change of FN was found due to the adsorption on BML-D_2O interface.

Immobilization of IgG on gold is an active research field for designing immunosensor for medical diagnostic purpose. The adsorption state of the IgG at the gold-solution interface was investigated by the NG-IRRAS. IgG was adsorbed on gold surfaces i.e. coated by the 16-mercaptohexadecanoic acid (MHA)-SAM and by the MHA-SAM activated by N-(3-dimethylaminopropyl)-N'-ethylcarbodiimide hydrochloride (EDC) and N-hydroxysuccinimide (NHS). It was also found that IgG was easily adsorbed on the PEG-coated prism surface in pure D_2O, while IgG adsorption on the PEG-coated

CaF_2 surface was suppressed sufficiently in NaCl/D_2O (140 mM) and D_2O based PBS solutions (Fig. 2b). I chose D_2O based PBS solution containing 140 mM NaCl for IRRAS measurement of IgG at the gold-solution interface.

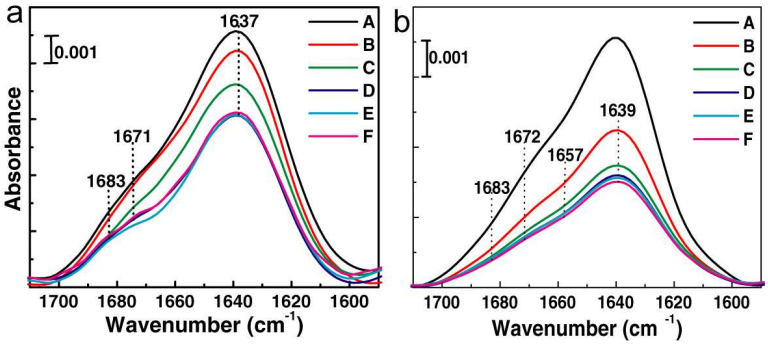

Fig. 3 The amide I bands of adsorbed proteins at solid-solution interface observed by the new NG-IRRAS.
a) Spectra of FN using pure D_2O as the solvent.
b) Spectra of IgG using NaCl (140 mM) added D_2O based PBS solution.
A) Spectra for protein injection and waiting 3 h (FN) and 30 min (IgG) for adsorption on solid surfaces,
Spectra were taken every after 0.5 ml D_2O solutions flushes; B) 0.50 ml C) 1.0 ml D) 1.5ml E) 2.0 ml, and F) 2.5 ml.

The IR spectra showed that IgG easily adsorbed on the MHA-SAM coated and activated-MHA-SAM coated gold surfaces. The conformation change of the IgG adsorbed on the MHA-SAM coated gold surface was ignorable when the IRRAS spectrum was compared with the FT-IR spectra of IgG dissolved in solution. Absorption spectra at the amide I band region of the IgG in the solution phase and at the solid-solution interface were measured with good reproducibility. The amide I band of the IgG molecule covalently bonded to the MHA-SAM (Fig. 3b) was quite similar to that of the IgG on the MHA-SAM coated gold surface. The covalent bond is formed between the COOH-terminated MHA-SAM and the lysine residue of the IgG. Because of lysine residue distributes almost homogeneously on the IgG surface, the covalently bonded IgG had random orientation similar to the physisorbed IgG on MHA-SAM coated gold surface.

After the solid-solution interface IRRAS experiments, the same substrates were examined in the vacuum IRRAS. The amide I band shape was significantly different from that in the solution for both FN and IgG. This change of amide band is due to the denaturation of the proteins during the removal of water from the substrate surface.

As a whole, I have succeeded for the first time in constructing a new NG-IRRAS system having 8 μm gap to flow reagent solution for monitoring the chemical reaction. A specially designed sample holder is used to keep the gap constant during the injection of the reagent solution within a certain injection speed. Adsorption of proteins on the prism surface, which interferes with precise measurement, is suppressed using PEG-coating of the prism surface and controlling the solution pH and the effects of the salt. The amide I bands of the IgG molecules dissolved in the solution and covalently bonded to the COOH-terminated SAM surface at solid-solution interface have been clearly recorded for the first time. This new IRRAS instrument can be easily applicable in the characterization of different antibody-antigen reactions on IR-reflective metal surfaces in physiological condition.

Contents

Chapter 1

Introduction

1.1 General principle of protein-solid interaction in aqueous solution

Spontaneous adsorption of protein at solid-solution interfaces has been extensively studied [1-54]. Protein interactions with solid surfaces involve a complex interplay of van der Waals force, hydrogen bonding, electrostatic force and hydrophobic interaction [8]. Previous studies of protein adsorption on solid surfaces showed that both hydrophobic and electrostatic interactions determine the amount of the adsorbed protein [9] and that the effect of the electrostatic interaction becomes more important when the adsorption is performed at low ionic strength where the screening effect of added salts is weakened [10].

Adsorption of protein at a solid-solution interface is not only dependent on the protein but also strongly influenced by the chemical and physical properties of the interface. In protein adsorption studies, various kinds of materials are used such as oxides, polymers, metals and minerals. On a hydrophobic surface, proteins strongly adsorbed with high surface coverage and with conformational change [11, 12]. To study the effect of surface chemistry on the degree of protein adsorption, the preparation of self-assembled monolayers (SAMs) provides an efficient way [13].

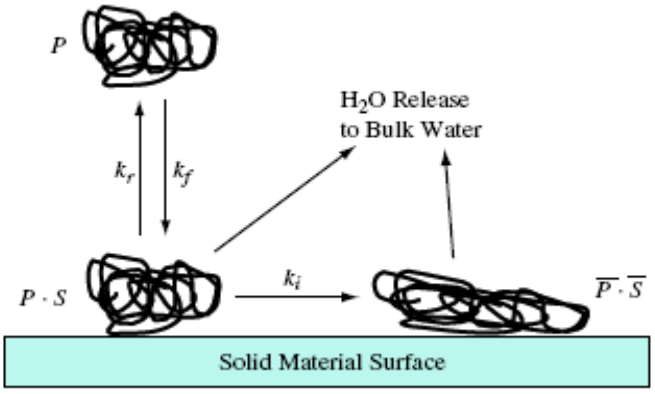

Figure 1.1 Schematic of the protein adsorption process at solid-aqueous solution interface [14].

A general illustration of protein adsorption process at solid-solution interface is shown in Figure 1.1. This protein adsorption process can also be explained by the following equilibrium equations [14]

$$P \cdot (m+n)\,H_2O + S \cdot (r+\upsilon)\,H_2O \underset{k_r}{\overset{k_f}{\rightleftharpoons}} P \cdot S \cdot (n+\upsilon)\,H_2O + (m+r)\,H_2O \quad \text{.....(1)}$$

$$P \cdot S \cdot (n+\upsilon)\,H_2O \xrightarrow{k_i} \overline{P} \cdot \overline{S} + (n+\upsilon)\,H_2O \quad \text{.....(2)}$$

P = concentration of protein in aqueous solution

S = concentration of active site of the surface

$P \cdot S$ = concentration of reversibly adsorbed protein on the active site of the surface

$\overline{P} \cdot \overline{S}$ = concentration of irreversibly adsorbed protein on the active site of the surface

k_f = forward reaction rate constant of reversible adsorption

k_r = reverse reaction rate constant of reversible adsorption

k_i = irreversible reaction rate constant of irreversible adsorption

Protein (P) reversibly adsorb on the active site of the surface (S) with a concentration ($P \cdot S$) from the solution with the reaction rate of k_f and k_r constants for the forward and

reverse reactions, respectively (eq. (1)). $\overline{P} \cdot \overline{S}$ is the concentration of irreversibly adsorbed protein on the active site of the surface with reaction rate constant of k_i for the transition of the reversibly adsorbed protein form to an irreversible bound state. Water molecules in or on the protein are released to bulk solution at various stages during the adsorption on surface.

A surface becomes saturated with the adsorbed protein if sufficient interaction time is provided because of the irreversible step of protein adsorption process (eq.(2)). The adsorbed protein layer is assembled on the surface through protein–surface and protein–protein interactions. In the protein adsorption process on the protein saturated surface, the irreversible step of the protein adsorption is decreased by the steric restrictions of the previously adsorbed protein due to the hydration shell on the protein. Thus, the proteins additionally adsorbed on the saturated protein layer were found in native and possibly in the reversible adsorbed state [15]. This behavior is frequently observed. A fraction of protein is found to desorb from an adsorbed protein layer during the following exposure of the surface to pure buffer solution while another fraction of the protein layer remains irreversibly adsorbed to the surface.

When a protein solution and a solid surface come in contact with each other, then the protein starts to absorb on the surface until saturation. In case of a hydrophobic surface, the protein is absorbed on its hydrophobic region. The protein unfold and spread its hydrophobic core over the surface owing to the thermodynamic driving force to reduce the net hydrophobic surface area of the system exposed to the aqueous solvent [16]. On hydrophilic surfaces, the protein adsorption is mainly dominated by the electrostatic interaction caused by the charged and polar functional groups of the protein surface [16]. The protein adsorption processes stop on the surface at the monolayer coverage, and then the further adsorption of protein induced by protein-protein interactions. The final organization of the adsorbed protein layer depends on the chemical and physical properties of the protein, the surface, and the aqueous solution, and the thermodynamics of the interactions between these system components [17]. Agnihotri and Siedlecki used tapping-mode atomic force microscopy (AFM) to observe time dependent structural

differences in fibrinogen adsorbed to hydrophilic (mica) and hydrophobic (graphite) surface [18]. In this study, four different orientational states of fibrinogen were observed on each surface. The height of the adsorbed protein on the hydrophobic surface decreased with time to a plateau value of ~1.0 nm, while the height increased to a plateau value of ~2.1 nm with time on the hydrophilic surface. And it was also observed that the AFM tip did not tend to move the protein on the hydrophobic surface, which indicates tight bounding between the protein and the hydrophobic surface.

1.2 Studies on protein adsorption at solid-solution interfaces

Protein adsorption on solid inorganic surfaces has received considerable interest in the research area for biosensor. Protein immobilization is not only carried out on flat bulk surfaces but also on nanoparticle surfaces [19-22, 42-44, 48-54]. Silicon and gold were extensively used in biomaterials research for their inactive characteristics; a few representative examples are introduced in this section.

Silicon is an excellent substrate material for biosensor devices, since advanced micro-fabrication technologies can be applied to integrate biosensors in electronic devices [23]. Silicon surface is covered by a native or an artificial silica layer, and various kinds of surface modification techniques have been used for the protein immobilization, e.g. hydrophilicity control [24], SAM formation [12], and grafting of ligand molecules such as biotin [25, 26]. The adsorption state of fibronectin (FN) on silica surface is an important issue, because FN coating is used as an extra cellular matrix for cell ion channel current measurement [27]. Human plasma FN absorption was studied on bare hydrophilic silica and a methylated hydrophobic silica surface [22]. In this experiment, on the hydrophilic silica surfaces 70% of the adsorbed FN molecules had an elongated structure with partial intramolecular chain interactions, compared to the FN molecules adsorbed on the methylated SiO_2 surfaces. Zangooie et al. investigated the adsorption of human serum albumin and fibrinogen on thermally oxidized porous silicon surface, which were used either as prepared or were hydrated in a deionized water bath prior to their use. The volume percentage of the adsorbed albumin decreased from 24% to 13%

due to the hydration and the amount of the adsorbed fibrinogen depending on the concentration in the solution [28]. Site-directed fluorescence labeled protein and silica nanoparticle were used to study protein-silica interaction [19]. In this report the author showed that the protein adsorption on silica nanoparticles is strongly pH-dependent; the adsorption is directed by positively charged areas on the protein surface toward the negatively charged silica surface. Lundqvist et al. investigated the influence of the silica particle curvature on the adsorption of Human carbonic anhydrase I (HCAI), and found that particles with a larger diameter lead to stronger particle-protein interaction. Testing of SiO_2, TiO_2 and polystyrene particles with various degree of surface carboxylation, together with protein and polyethylene glycol surface coatings, showed that cellular associations and protein binding both strongly depend on the particle surface chemistry [29].

Adsorption of proteins on solid surfaces was investigated from both view points of adsorbed amount and conformational changes. The AFM [30, 31] and radiolabelling [32, 33] techniques can be used to get information of individual protein molecules on surfaces. AFM and X-ray at grazing incidence angles strongly showed that globular protein GlnB-Hs deposited on Si (111) by spin-coating forms circular 100 nm to 150 nm wide face-up donut shaped protein aggregates [34]. GlnB-Hs protein crystal domains formed along perpendicular direction on Si surface during the spin coating and these domains could play a role on nucleation for crystal growth and stimulate crystallization of reluctant proteins. The electrostatic interaction between proteins and substrate surfaces was studied using a positively charged SAM of 3-aminopropyl-triethoxysilane (APTES) layer and moderately negative ferritin, Fer-4 (horse-spleen-ferritin L subunit lacking four amino acid residues from the N-terminus) and it was proven that protein adsorption density depends on the quantitative balance of surface charge on the substrate and protein [35]. A structural analysis of a monoclonal immunoglobulin G (IgG) adsorbed on variously modified silica surfaces (bare hydrophilic, methylated hydrophobic, and triblock-copolymer coated hydrophobic) was performed using attenuated total internal reflection infrared (ATR-FTIR) spectroscopy using the oxide layer on a silicon cylindrical internal

reflecting element [12, 36]. The adsorption-induced reduction in the β-sheet content in IgG was observed both on the methylated hydrophobic surfaces and on the bare hydrophilic silica surfaces, although the reduction degree is larger on the former surface [12]. However, such adsorption-induced deformation of IgG on the hydrophilic silica surface was not observed in ref. 36. IR reflection absorption spectroscopy (IRRAS) which selectively detect vibrational mode perpendicular to the surface indicated the uniform orientation of covalently immobilized avidin on a flat COOH-modified silica surface [25].

Gold is chemically and biologically inert metal, and especially important substrate materials for biosensors and biochips such as protein chips [37, 38] and DNA chips [39-41]. Gold nanoparticles coupled with bimolecules have become increasingly important in the biological nanoprobe researches [42–44, 48-54]. A new method has been developed for the preparation of amine-terminated surfaces with a highly cross-linked Si–O–Si network sub-layer on gold substrates to bind avidin through biotin bond [45]. Terrettaz et al. showed that a matrix porin OmpF of *Escherichia coli* is suitable for interaction with flat gold and semiconductor surfaces [40]. An efficient strategy for immobilizing proteins on a gold surface was developed by employing the gold binding polypeptide (GBP) [46, 47]. Antibody molecules immobilized on B5C1-thiol modified gold surface, and they bind to the corresponding antigen effectively with high orientation [46]. Antibody human IgG complexes were formed via thiol chemistry on 20-nm-thick gold islands, which deposited on the surface of IR-transparent Ge-containing chalcogenide glass films [47].

Gold nanoparticles, especially colloidal golds, are promising material for the surface-enhanced IR absorption spectroscopy (SEIRA) [48]. Immunolabeling efficiency of protein A to colloidal gold particles was studied by varying the particle diameter in the range of 5-16 nm in various protein concentrations [49]. The Cytochrome C (Cyt-c) coated gold nanoparticles were used as colorimetric sensor for the detection of protein conformational change, which is observed by surface plasmon resonance (SPR) at different pH [50]. An enormous and continuous SPR angle shift of the gold particles was observed when cytochrome b-562 is adsorbed on the nano gold surface [51]. The GBP

was also employed for the immobilization of proteins on a gold surface [52]. The conformational changes of cyclohexanethiol (CHT) on gold nanoparticles and on gold plate surfaces were investigated on molecular-scale by scanning tunneling microscope, and it was found that there were two axial and equatorial conformers in the CHT monolayer on an Au (111) surface as meta-stable conformers [53]. Triulzi et al. studied the effect of laser radiation to the amyloid β (Aβ) conjugate-gold nanoparticles and reported that monofunctional gold nanoparticles coupled which Aβ conjugates destroyed the aggregates of Aβ by the photothermal ablation [54].

1.3 Purpose and brief summary of this study

The adsorption of protein on the surfaces and the conformational changes due to the adsorption have been characterized and monitored using various techniques, as described in the previous section. IR spectroscopy is a powerful method to detect the structural change of the adsorbed proteins. Several IR techniques have been used to observe the protein at different conditions, such as in water, at the air-water interface, on solid surfaces, and at solid-solution interface. IR-transparent materials were generally used in the previous IR studies at solid-solution interfaces, and there are very few IR systems for the adsorbate or biomaterial reaction at the interface between IR-non-transparent materials and solutions. An aqueous solution layer is necessary on the non-transparent solid surface to observe biomaterials at the solid-solution interface. But water has strong absorptivity in the IR region and water layer causes a significant noise of the baseline. This is the reason that very few number of IRRAS experimental configuration have been reported. In the reported narrow gap IRRAS (NG-IRRAS), the solution layer is too thin (1~2 μm) for monitoring chemical reactions, and it is not easy to increase this layer thickness and inject solutions. Injections of a reagent solution into the narrow solution layer easily change the solution layer thickness, which causes a significant distortion of the baseline. Therefore, I have constructed a new IRRAS system having 8 μm gap for the observation of adsorbed biomaterials at the solid-solution interface, and succeeded for the first time to control the water layer thickness during the injection of reagent solution with

nanometer level fluctuation.

In chapter 2, principle for narrow gap solid-solution interface IRRAS (NG-IRRAS) and the surface selection rule are described. The IR incident angle on CaF_2 prism surface is calculated using the H_2O refractive index at CaF_2/H_2O interface to avoid total internal reflection.

The construction process of the NG-IRRAS is presented in chapter 3. The detailed construction steps using a JEOL JIR-7000 FT-IR spectrometer and a home built sample chamber system are described. The structure of sample holders for the IRRAS measurement at solid-solution interface studies and in vacuum are described.

Chapter 4 is the experimental section of this thesis. In this section, the cleaning protocol of the silicon substrate with a buried metal layer (BML) and of gold substrates and solution preparation methods are described. The detail about the surface modification of a CaF_2 prism base with 2-methoxy-(polyethylene) oxypropyltrimethoxysilane (PEG), and the formation and activation of 16-mercaptohexadecanoic acid (MHA)-SAM on the gold surface are depicted.

In chapter 5, the origins of the baseline distortions and their removal are described. The effects of temperature, solution injection flow, and adsorbed water on optical components on baseline are explained. Optimization of every factor is discussed briefly.

In chapter 6, the application of this new NG-IRRAS is presented. In this section, protein adsorption on the CaF_2 prism surface and the prevention of the adsorption by PEG-coating and the effects of the solution pH and salt concentration are described. The amide I bands of the IgG molecules dissolved in the solution, and the IgG covalently bonded to the COOH-terminated SAM surface are circumstantially discussed.

Chapter 7 is the summary of this thesis.

References

[1] Y. Ikada, Adv. Polym. Sci. 57 (1984) 103.

[2] E. R. Baier, E. A. Meyer, R. J. Natiella, R. R. Natiella, M. J. Carter, J. Biomed. Mater. Res. 18 (1984) 337.

[3] M. Malmsten (ed.), Biopolymers at interfaces, Marcel Dekker, New York (2003).

[4] A. Baszkin and W. Norde (eds.), Physical chemistry of biological interfaces, Marcel Dekker, New York (2000).

[5] T. A. Horbett and J. L. Brash (eds.), Proteins at interfaces II, American Chemical Society, Washington, DC (1995).

[6] J. L. Brash and T. A. Horbett (eds.), Proteins at interfaces, American Chemical Society, Washington, DC (1987).

[7] J. D. Andrade (ed.), Surface and interfacial aspects of biomedical polymers, Vol. 1 and 2, Plenum Press, New York (1985).

[8] H. Elwing, S. Welin, A. Askendal, R. U. Nilsson, J. I. Lindstrom, J. Colloid Interface Sci. 119 (1987) 203.

[9] W. Norde, Adv. Colloid Interface Sci. 25 (1986) 267.

[10] J. L. Ortega-Vinuesa, M. J. G´alvez-Ruiz, R. Hidalgo-Alvarez, Langmuir 12 (1996) 3211.

[11] S.-S. Cheng, K. K. Chittur, C. N. Sukenik, L. A. Culp, and K. Lewandowska, J. Colloid Interface Sci., 162 (1994) 135.

[12] J. Buijs, and W. Norde, Langmuir 12 (1996) 1605.

[13] K. L. Prime and G. M. Whitesides, Science 252 (1991) 1164.

[14] W. Norde, C. A. Haynes, Reversibility and the mechanism of protein adsorption. In Proteins at Interfaces II. Fundamentals and Applications; Horbett, T.A., Brash, J.L., Eds.; American Chemical Society: Washington, DC, (1995) 26.

[15] C. F. Wertz, M. M. Santore, Langmuir 18 (2002) 706.

[16] C. F. Wertz, M. M. Santore, Langmuir 17 (2001) 3006.

[17] J. Talbot, G. Tarjus, P. R. Van Tassel, P. Viot, Colloids Surf. A. 165 (2000) 287.

[18] A. Agnihotri, C.A. Siedlecki, Langmuir 20 (2004) 8846.

[19] M. Karlsson, U. Carlsson, Biophys. J. 88 (2005) 3536.

[20] M. Lundqvist, I. Sethson, B.-H. Jonsson, Langmuir 20, (2004) 10639.

[21] J. C. Orendorff, A. Gole, K. Tapan, Sau, J. C. Murphy, Anal. Chem. 77 (2005) 3261.

[22] J. Kneipp, H. Kneipp, W. L. Rice, K. Kneipp, Anal. Chem.77 (2005) 2381.

[23] M. Goryll, S. Wilk, G.M. Laws, T. Thornton, S. Goodnick, M. Saraniti, J. Tang, R.S. Eisenberg, Superlattice Microst. 34 (2003) 451.

[24] M. Bergkvist, J. Carlsson, S. Oscarsson, J. Biomed. Mater. Res. 64A (2003), 349.

[25] N. Misawa, S.Yamamura, Y.-H. Kim, R. Tero, Y. Nonogaki, T. Urisu, Chem. Phys. Lett. 419 (2006) 86.

[26] Z. Liu, M. D. Amiridis, Surf. Sci. 596 (2005) 117.

[27] T. Urisu, T. Asano, Z.-L. Zhang, H. Uno, R. Tero, H. Junkyu, I. Hiroko, Y. Arima, H. Iwata, K. Shibasaki, M. Tominaga, Anal Bioanal. Chem. 391 (2008) 2703.

[28] S. U. Zangooie, R. Bjorklund, H. Arwin, Thin Solid Films, 313 (1998) 825.

[29] M. Ehrenberg, J. L. McGrath, Acta Biomater. 1 (2005) 305.

[30] L. Haggerty, A. B. Watson, A. M Bateau, M. A. Lenhoff, J. Vac. Technol. B, 9 (1991) 1219.

[31] A. C. Siedleecki, J. S. Eppell, E. R. Marchant, J. Biomed. Mater Res. 28 (1994) 971.

[32] M. S. Slack, A. T. Horbett, J. Colloid Interface Sci. 133 (1989) 148.

[33] M. S. Slack, A. T. Horbett, J. Colloid Interface Sci. 124 (1988) 533.

[34] A. F. Lubambo, E. M. Benelli, I. Mazzaro, F. Yokaichyia, C. Giles, P. Ce´sar de Camargo, Macromol. Symp. 245 (2006) 140.

[35] K. Yamada, S. Yoshii, S. Kumagai, I. Fujiwara, K. Nishsio, M. Okuda, N. Matsukawa, I. Yamashita, Jpn. J. Appl. Phys. 45 (2006) 4259.

[36] C.E. Giacomelli, M.G.Bremer, W. Norde, J. Colloid Interface Sci. 220 (1999) 13.

[37] S. Watanabe, K.Usui, K. Tomizaki, K. Kajikaw, H. Mihara, Mol. Biosyst. 1(2005) 363.

[38] K.-Y. Park, M.-S. Kim, S.-Y. Choi, Biosens. Bioelectron. 20 (2005) 2111.

[39] S. Takenaka, K. Yamashita, M. Takagi, Y. Uto, H. Kondo, Anal. Chem. 72 (2000) 1334.

[40] Z. Wan, Y. Wang, S. S. Li, L. Duan, J. Zhai, Biochem. Mol. Biol. Int. 38, (2005) 399.
[41] J. B. Fiche, A. Buhot, R. Calemczuk, T. Livache, Biophys. J. 92 (2007) 935.
[42] M. C. Daniel, D. Astruc, Chem. Rev.104 (2004) 293.
[43] E. Katz, I. Willner, Angew. Chem. Int. Ed. 43 (2004) 6042.
[44] C. M. Niemeyer, Angew. Chem. Int. Ed. 40 (2001) 4128.
[45] S. Terrettaz, W. P. Ulrich, H. Vogel, Q. Hong, L. G. Dover, J. h. Lakey, Protein Sci. 11 (2002) 1917.
[46] S. Kanno, Y. Yanagida, T. Haruyama, E. Kobatake, M. Aizawa, J. Biotechnol. 76 (2000) 207.
[47] C. Yu, A. Ganjoo, H. Jain, C. G. Pantano, J. Irudayaraj, Anal. Chem. 78, (2006) 2500.
[48] A. J. Seelenbinder, W. C Brown, P. Pivarnik, G. A. Rand, Anal. Chem.71 (1999) 1963.
[49] L. Ghitescu, M. Bendayan, J. Histochem. Cytochem.11 (1990) 1523.
[50] S. Chah, M. R. Hammond, R. N. Zare, Chemistry & Biology, 12 (2005) 323.
[51] H. S. Zhou, S. Aoki, I. Honma, M. Hirasawa, T. Nagamune, H. Komiyam Chem. Commun. (1997) 605.
[52] T. J. Park, S. Y. Lee, S. J. Lee, J. P. Park, K. S. Yang, K.-B. Lee, S. Ko, J. B. Park, T. Kim, S. K. Kim, Y. B. Shin, B. H. Chung, S.-J. Ku, D. H. Kim, I. S. Choi, Anal. Chem. 78 (2006) 7197.
[53] S.-W. Joo, H. Chung, K. Kim, J. Noh, Surf. Sci. 601 (2007) 3196.
[54] R. C. Triulzi, Q. Dai, J. Zoub, R. M. Leblanc, Q. Gud, J. Orbulescu , Q. Huo, Colloids Surf. B 63 (2008) 200.

Chapter 2

Surface selection rule and principle of narrow gap solid-solution interface IRRAS

2.1 Fourier-transform infrared spectroscopy at solid-solution interface

At solid-solution interfaces adsorption and desorption occur frequently. Adsorption and desorption are the fundamental processes of many phenomena such as dissolution, detergency, corrosion and corrosion inhibition, adhesion, flotation, chromatography etc. The adsorption-desorption equilibrium, kinetics and reaction mechanisms at the solid-solution interfaces are attractive scientific research targets. To understand the chemistry of surfaces in liquid environments, many experimental techniques including infrared spectroscopy are used for exploring the real time characteristics.

Fourier-transform infrared spectroscopy (FT-IR) is a powerful technique to analyze surface architecture and adsorbates on surfaces. This method has an advantage that the organic contents of biological samples can be analyzed without any modification or labeling. To understand the properties of adsorbed biomaterials on metal surfaces in different conditions, several IR-based techniques have been developed. The increasing importance of FTIR in surface science is due to the recent advancement of instrumentation in sensitivity and speed of measurements. Although the instrumental advances play an important role, understanding the origin of physical processes governing spectral detection and interpretation of vibrational spectra are also necessary.

FTIR spectroscopy has been widely used for the study of biomaterials on the solid surface under the vacuum condition [1-5]. There are two major IR experimental set-ups to study solid surface and adsorbates: attenuated total (internal) reflection (ATR-IR) and reflection absorption spectroscopy (RAS). Only limited numbers of IR [6-11] techniques are available for the investigation of adsorbate at the solid-solution interface.

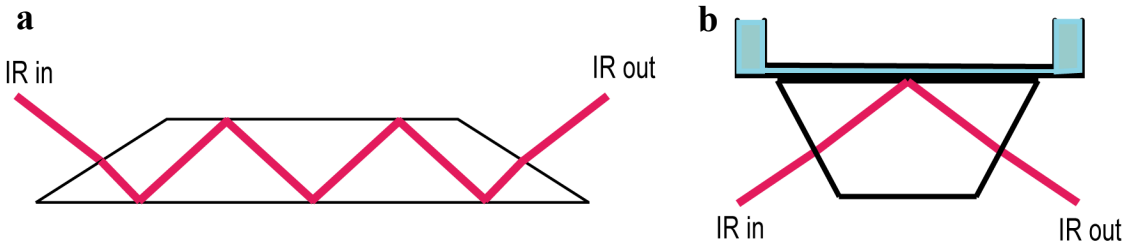

Figure 2.1 Arrangement of the light path in ATR-IR systems a) Conventional ATR-IR, and b) Kretschmann ATR

transparent metal surfaces under solution [8-11]. In the conventional ATR-IR, the IR beam is introduced into the prism and is incident on the surfaces of the prism at an angel greater than the critical angel of the total reflection. If the geometry of the experiment is correctly arranged, then multiple internal reflections occur as shown in Figure 2.1a. Kretschmann ATR configuration is also used as another total-reflection type IR technique (Figure 2.1b) [11]. These methods are highly sensitive, but only IR-transparent materials, for example SiO_2, Ge, ZeSe, ZnS, KRS-5 and AMTIR (amorphous material transmitting infrared radiation) crystals are used as a substrate in the ATR technique. In ATR-IR, thick adsorbed sample can not be measured due to the limited penetration of evanescent IR wave at the crystal interface. The reported penetration depth of germanium is less then 1 μm [12].On the other hand, the IRRAS method gives high resolution and high sensitivity on the reflective metal surfaces [5, 13]. Only a few IRRAS systems were reported for observing adsorbate at solid-solution interface on non-transparent metal using very thin gap (1-2 μm) [6, 7].

To overcome these disadvantages, I developed a new narrow gap reflection absorption spectroscopy (NG-IRRAS) system to investigate biomaterials at the solid-solution interface in my doctoral course work.

2.2 Surface selection rules for IRRAS

The incident IR radiation on a surface can be split into s-polarized and p-polarized components of the electric field (Figure 2.2a). For the s-polarized component, the electric field vector oscillates in the plane perpendicular to the plane of incidence.

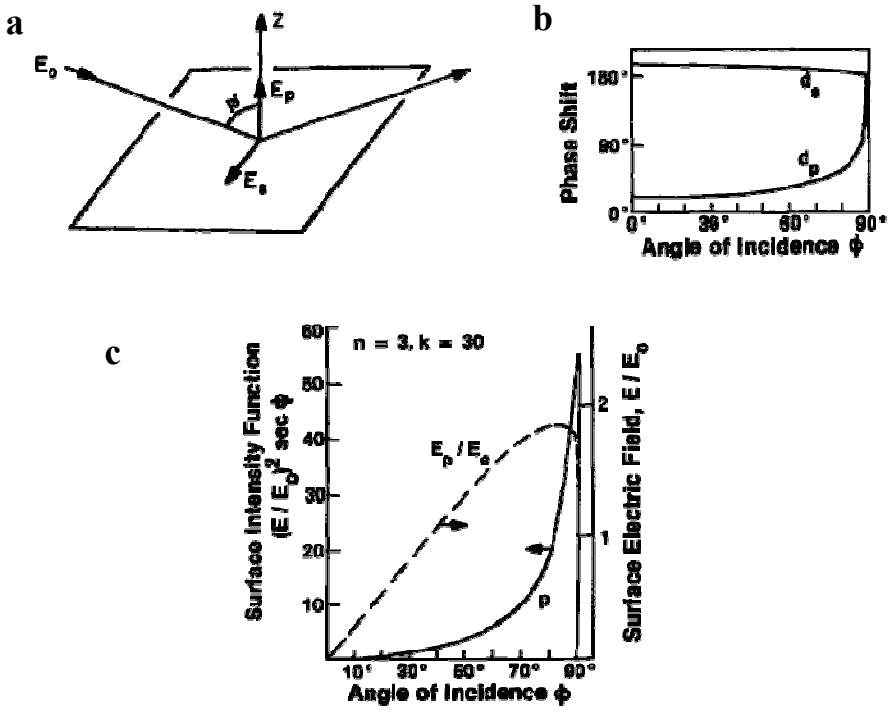

Figure 2.2 a) Reflection of light on a clean metal surface, the electric field denoted Ep and Es. b) Phase shift of light; dp and ds versus angle of incident, c) electric field and intensity of P-light versus angle of incident [14, 15]

As the electrical conductivity of a metal is very high in the infrared region, the electric field component tangential to the surface is zero at the surface. The phase of the light changes 180° before and after the reflection at a metal surface, and this phase inversion leads to vanishing resultant amplitude of the electric field vector at the surface (Figure 2.2b).Therefore, the s-polarized component does not have effective contribution to the

excitation of the vibrating dipoles at the surface. As a result, vibrational modes parallel to the substrate surface are not detected in IRRAS. The electric field vector of the p-polarized radiation oscillates in the plane of incidence. Its intensity at the surface becomes even higher than that of the incident beam depending on the angle of incidence (Figure 2.2c). The p-polarized radiation can interact with molecular vibrations which have a non-zero component of the dipole moment derivative normal to the surface. Thus, p-polarized light is effective in IRRAS on metal surfaces. This is the origin of surface selection rule of IRRAS, which states that only the perpendicular component of the vibrational dipole moment is active [16,17]. Thus, the absorbance spectra of biomaterials at the solid-solution interface are given mainly from the contribution of p-polarized radiation, if the biomaterials layer is sufficiently thin compared with the IR wavelength.

2.3 Incident angle calculation

In the present solid-solution interface IRRAS system, CaF_2 prism is used to introduce the IR beam to the sample surface. If the incident angle of light is higher than the critical angle then total internal reflection (TIR) occurs at the CaF_2/solution interface and the IR beam does not reach to the sample surface. The critical angle of CaF_2/ H_2O system was calculated using Snell's equation,

$$n_1 \sin\theta_i = n_2 \sin\theta_r$$

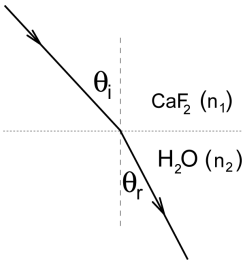

n_1=refractive index of CaF_2
n_2=refractive index of H_2O
θ_i=incident angle of IR
θ_r=refractive angle of IR

The definition of the critical angle for the total reflection (θ_{crtc}) is θ_r=90°; so the equation is

$$n_1 \sin\theta_{crtc} = n_2 \sin 90°$$

$$\sin\theta_{crtc} = n_2 / n_1$$

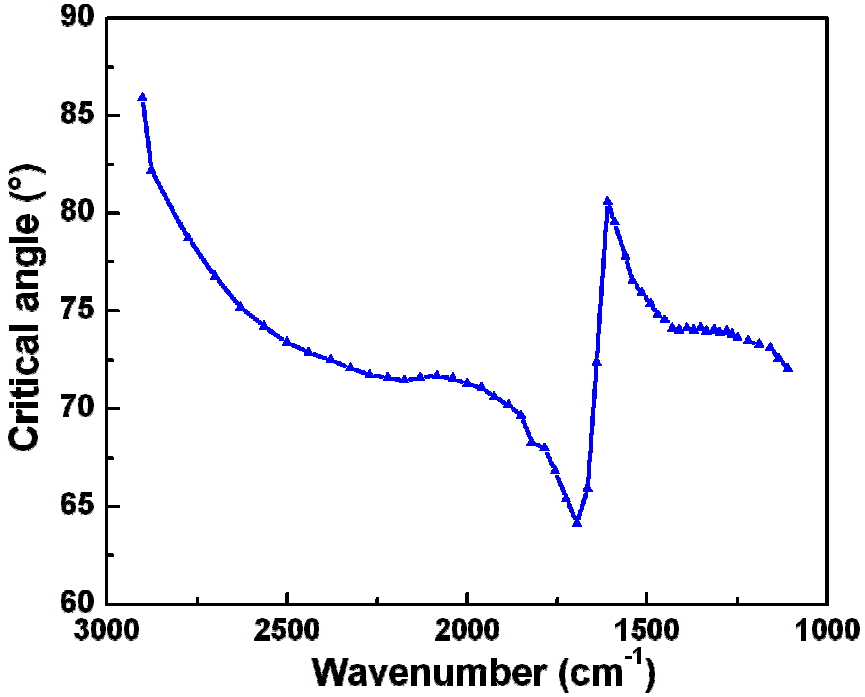

Figure 2.3 Dependence of critical angle of the total reflection at the CaF_2/ H_2O interface on the light wavenumber.

The dependences of θ_{crtc} on the light wavenumber were calculated using refractive index of CaF_2 (Appendix II) and H_2O (Appendix III) at the region of 1100 to 3000 cm^{-1} and shown in Figure 2.3.

Figure 2.3 shows that the lowest critical angle is 64.15° at 1695 cm^{-1}. Most of the IR light illuminates on the substrate surface through the H_2O layer if the incident angle of the IR is adjusted just below the critical angle. Therefore, in this new NG-IRRAS system the incident angle was set at 64°.

2.4 Principle of solid-solution interface IRRAS

Figure 2.4 shows the schematic of a solid-solution interface with adsorbates (CaF_2/D_2O/biomaterials/Au) which is used for the present IRRAS experiments. In this spectroscopic system a silicon wafer with buried metal layer (BML) substrate made by the wafer-bonding method, which has the structure of *SiO_2 (100)/$CoSi_2$/ Si(100)* [13], and a commercial gold substrate made by the sputter deposition on the Cr-pre-coated glass substrate (*Au/ Cr / glass;* Moritex Co. Tokyo, Japan) are used.

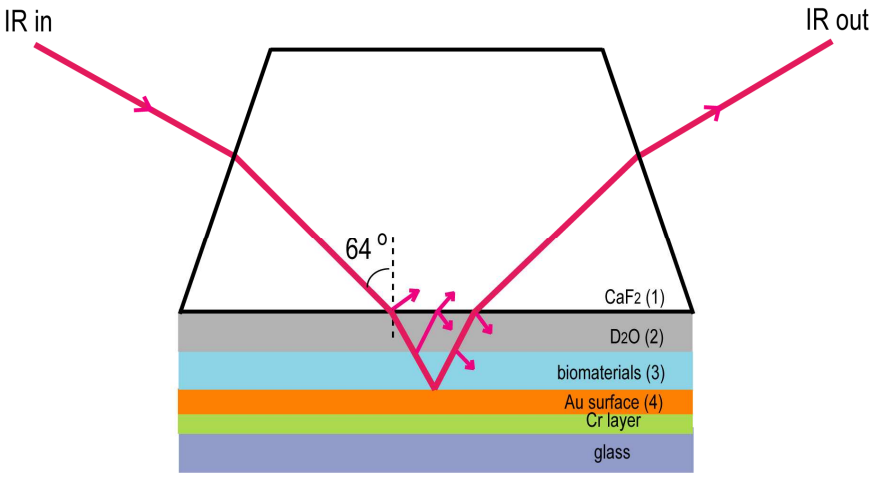

Figure 2.4 The schematic of the sample holder in the present IRRAS experiment. Layers 1-4 represent the CaF_2 prism, D_2O layer, adsorbed biomaterials layer and gold layer respectively.

It is assumed that the four layers CaF_2, D_2O, adsorbate and Au are isotropic, homogeneous, and parallel to each other. These layers are represented by layers 1-4, in Figure 2.4. The interaction of the IR light with the surface is described by the Fresnel equation, which incorporates the appropriate boundary conditions in the electromagnetic wave equations of the incident, reflected, and refracted wave.

If using the complex refractive index, $n_x=n_x-ik_x$, and the incident and the refractive angle Φ_i and Φ_r, the electric field reflectance r_{xy} at the interface of medium x and y(y=x+1) is given by

$$r_{xy} = -\frac{n_x \cos\Phi_r - n_y\cos\Phi_i}{n_x \cos\Phi_r + n_y\cos\Phi_i}$$

Thus,

$$r_{12} = -\frac{n_1 \cos\Phi_2 - n_2\cos\Phi_1}{n_1 \cos\Phi_2 + n_2\cos\Phi_1}$$

$$r_{23} = -\frac{n_2 \cos\Phi_3 - n_3\cos\Phi_2}{n_2 \cos\Phi_3 + n_3\cos\Phi_2}$$

$$r_{34} = -\frac{n_3 \cos\Phi_4 - n_4\cos\Phi_3}{n_3 \cos\Phi_4 + n_4\cos\Phi_3}$$

On the other hand, the electric field reflectance at the surface of the three layers 2, 3 and 4 (r_{234}) is obtained as follows

$$r_{234} = \frac{r_{23} + r_{34} * e^{-2i\Delta_3}}{1 + r_{23} * r_{34} * e^{-2i\Delta_3}}$$

,where Δ_3 is the phase shift of the light expressed as follows

$$\Delta_3 = \frac{2\pi}{\lambda} d_3 n_3 \cos\Phi_3$$

,where d_i represents the thickness of the layer i; and $\cos\Phi_i$ can be express as

$$\cos\Phi_3 = \sqrt{1-(\frac{n_2}{n_3}\sin\Phi_2)^2}$$

In the similar way, the electric field reflectance of four layers, 1, 2, 3, and 4 (r_{1234}) is obtained as follows

$$r_{1234} = \frac{r_{12} + r_{234} * e^{-2i\Delta_2}}{1 + r_{234} * r_{12} * e^{-2i\Delta_2}}$$

$$\Delta_2 = \frac{2\pi}{\lambda} d_2 n_2 \cos \Phi_2 \quad \text{and} \quad \cos \Phi_2 = \sqrt{1 - (\frac{n_1}{n_2} \sin \Phi_1)^2}$$

The absorbance of IR can be calculated as follows,

$$R_1 = \left| r_{1234} \right|^2 \quad (d3 \neq 0)$$

$$R_0 = \left| r_{1234} \right|^2 \quad (d3 = 0)$$

where, R_1 and R_0 are the reflectance from the IR beam with and without adsorbates, respectively, and correspond to the signal and back ground spectra in the IRRAS measurement. The absorbance of the adsorbate (A) is calculated as follows.

$$A = -\log \frac{R_1}{R_0}$$

References

[1] D.L. Allara, J.D. Swallen, J. Phys. Chem. 86 (1982) 2700

[2] D. F. Cui, V. A. Howarth, M. C. Petty, Thin Solid Films, 192 (1990) 391.

[3] J. L. Coutre, L. R. Narasimhan, C.K. Patel, H. R. Kaback, Proc. Natl. Acad. Sci. 94,(1997) 10167.

[4] Z. Liu, M. D. Amiridis, Surf. Sci. 596 (2005) 117.

[5] N. Misawa, S. Yamamura, Y.-H. Kim, R. Tero, Y. Nonogaki, T. Urisu, Chem. Phys. Lett. 419 (2006) 86.

[6] H. Seki, K. Kunimatsu, W. G. Golden, Appl. Spectrosc. 39, (1985) 437.

[7] D. D. Popenoe, S. M. Stole, M. Porter, Appl. Spectrosc, 46, (1992) 79.

[8] S.-S. Cheng, K. K. Chittur, C. N. Sukenik, L. A. Culp, K. Lewandowska, J. Colloid Interface Sci. 162, (1994) 135

[9] M. C. Hull, L. R. Cambrea, J. S. Hovis, Anal. Chem, 77 (2005) 6096.

[10] S. J. McClellan, E. I. Franses, Colloids and Surfaces A: Physicochem. Eng. Aspects, 260 (2005) 265.

[11] S. Morita, M. Tanaka, Y. Ozaki, Langmuir, 23 (2007) 3750

[12] K.K. Chittur, Biomaterials 19 (1998) 357.

[13] S. Yamamura, S. Yamuchi, S. Watanabe, M. Tabe, T. Kasai, Y. Nonogaki, T. Urisu, Jpn. J. Appl. Phys. 42, (2003) 3942.

[14] F. M. Hoffmann, Surf. Sci. Reports 3 (1983) 107.

[15] J. Pritchard, in: Vibrations in adsorbed layers, Conference Record Series of KFA, Eds. H. Ibach and lehwald (KFA, Julich, 1978), 114

[16] R. A. Dluhy, S. M. Stephens, S. Widayati, A. D. Williams, Spectrochim. Acta Part A 51 (1995) 1413-1447

[17] H. A. Pearce, N. Sheppard, Surf. Sci. 59 (1976) 205.

[18] R. A. Dluhy, J. Phys. Chem. 90 (1986) 1373.

Chapter 3

Construction of new narrow gap infrared reflection absorption spectroscopy (NG-IRRAS)

Chem. Phys. Lett. 466 (2008) 235.

3.1 Introduction

Infrared reflection absorption spectroscopy (IRRAS) techniques are used for detection of biomaterials on IR-non-transparent solid surfaces. A large number of IRRAS studies have been carried out on biomaterials at interfaces e.g. proteins and lipid membranes at the vacuum/solid [1-4] and air/water [5-7] interfaces. Polarization-modulation IRRAS was used to study such biomaterials at the interface between the solid surface and aqueous solution [8-12]. To detect biomaterials at the interface between solutions and IR-transparent metal surfaces, the conventional or Kretschmann type attenuated total internal reflection spectroscopy (ATR–IR) optical arrangements (Figure 2.1 in Chapter 2) are used. But the ATR is not available to the IR-non-transparent substrates [13, 14]. IRRAS is a single refection system, and the substrate is usually set in vacuum or water-vapor-free environments as shown in Figure 3.1a. The IR beam is directly irradiated on a sample surface and the reflected beam is guided to the detector [1-4]. On the other hand, to observe biomaterials at the solid-solution interface, the solution layer is necessary on the non-transparent solid surface. The water layer is essentially necessary for biomaterials to keep their life functions and the important amide bands of proteins appear around 1400-1700 cm^{-1}, where strong absorption band of water also exists. This strong absorption by water layer also causes a significant noise of the baseline. These are the main reasons that

very few numbers of IRRAS configurations have been reported about the biomaterials at the solid-solution interface (Figure 3.1b) [15, 16]. In these reported IRRAS systems, very thin (1~2 μm) solution layer was sealed between the substrate and the prism surface and solution could not be exchanged, and the spectra of the adsorbates were obtained by substituting those of the bare substrate [14].

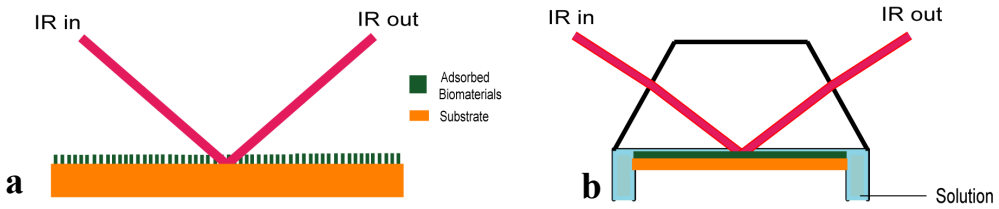

Figure 3.1 The reported optical configurations of a) vacuum IRRAS and b) conventional narrow gap-solid solution interface IRRAS

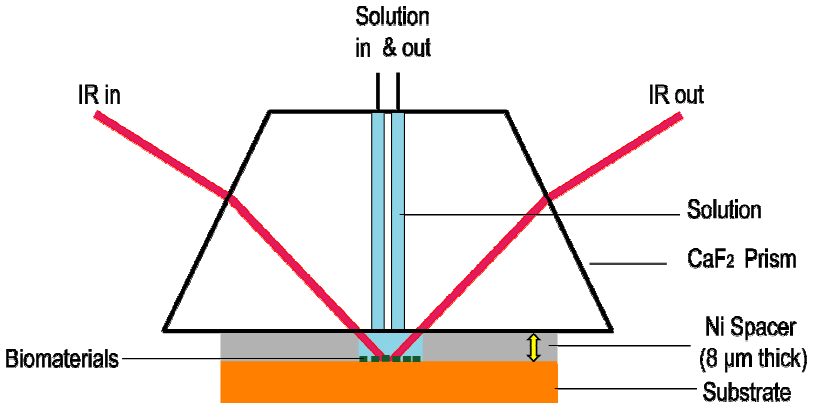

Figure 3.2 The optical configuration for the new narrow gap solid-solution NG-IRRAS in the present study

For the in-situ observation of the adsorbed biomaterials at the solid-solution interface using IRRAS technique, an injection system with a large gap between the prism and the substrate is necessary to make the reagent solution flow in and out of the sample holder.

No IRRAS system equipped with such a flow system has been reported to my knowledge. Considering these points, I have proposed a new narrow gap IRRAS (NG-IRRAS) system as shown in Figure 3.2, which was designed to observe the adsorption and reaction of biomaterials at the solid-solution interface.

3.2 New narrow gap infrared reflection absorption spectroscopy configuration and construction

The detail of the schematic experimental configuration of the new NG-IRRAS system is shown in Figure 3.3. The NG-IRRAS system consists of two parts. One is the IR source, for which a commercial JEOL JIR-7000 FT-IR spectrometer is used. The other is a home built sample chamber system consisting of mirror chambers, a sample chamber and a detector chamber.

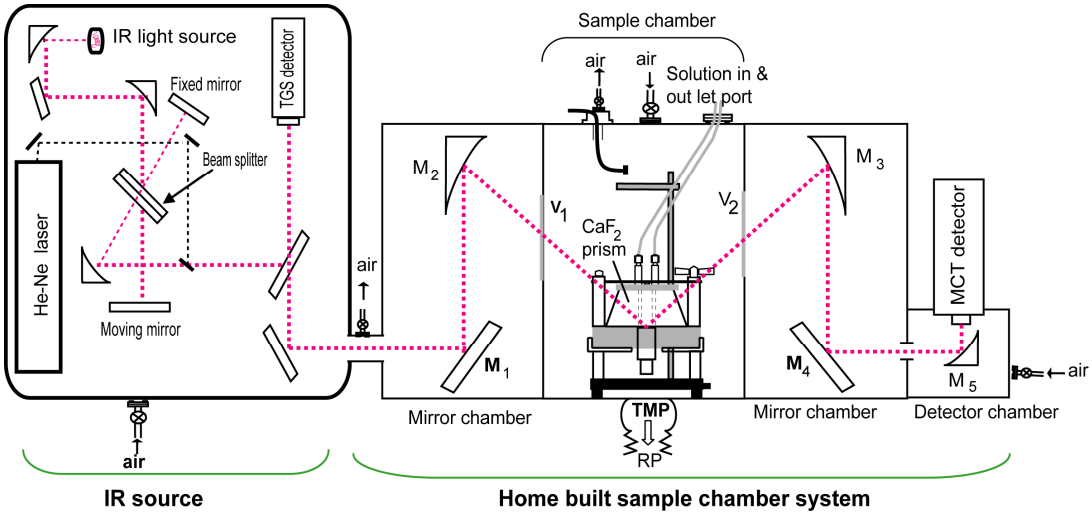

Figure 3.3 The outline of the experimental configuration of the new NG-IRRAS

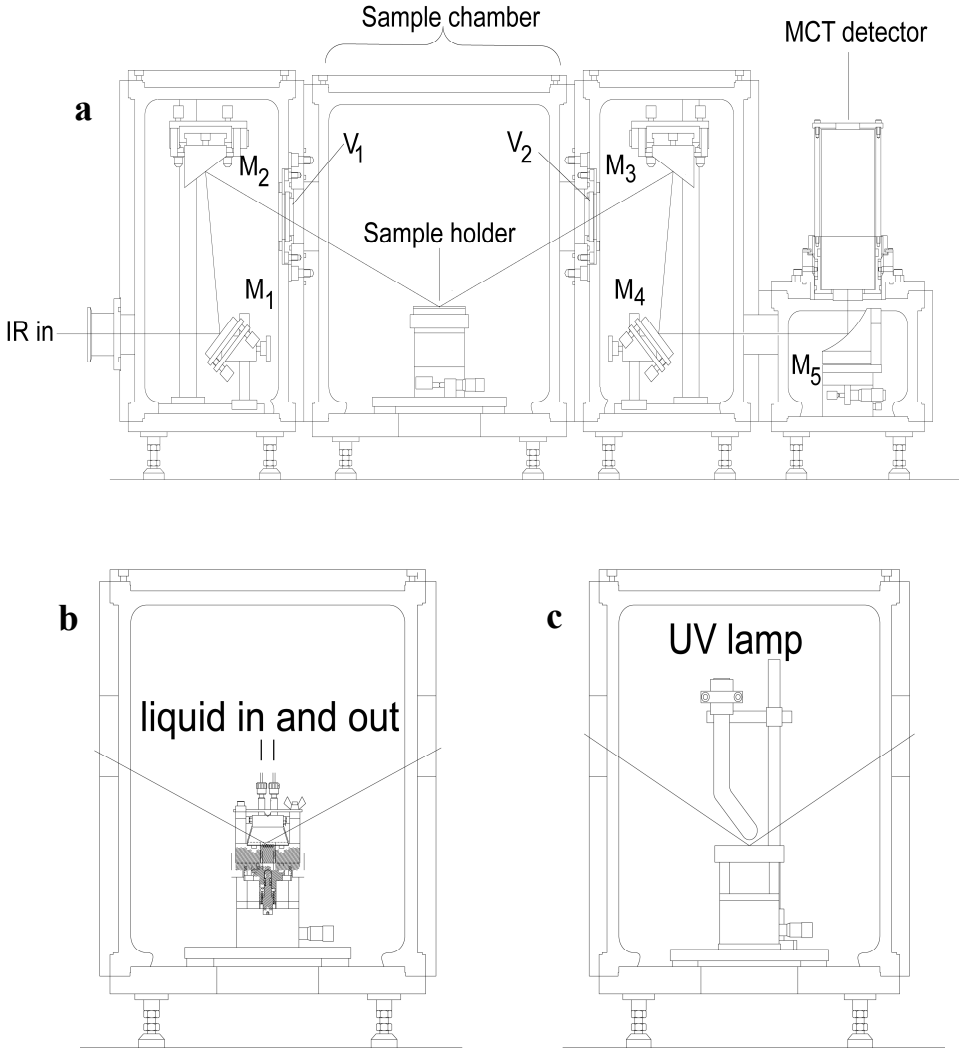

Figure 3.4 Schematic diagram of the sample chamber system for the new NG-IRRAS. a) Optical setup; M_1 and M_4: Al-coated plane mirrors, M_2, M_3 and M_5: Off-axis Au-coated paraboloidal mirrors; V_1 and V_2: CaF_2 window. b) Sample holder arrangement for IRRAS measurement at the solid-solution interface. c) Sample holder arrangement for IRRAS measurement in vacuum.

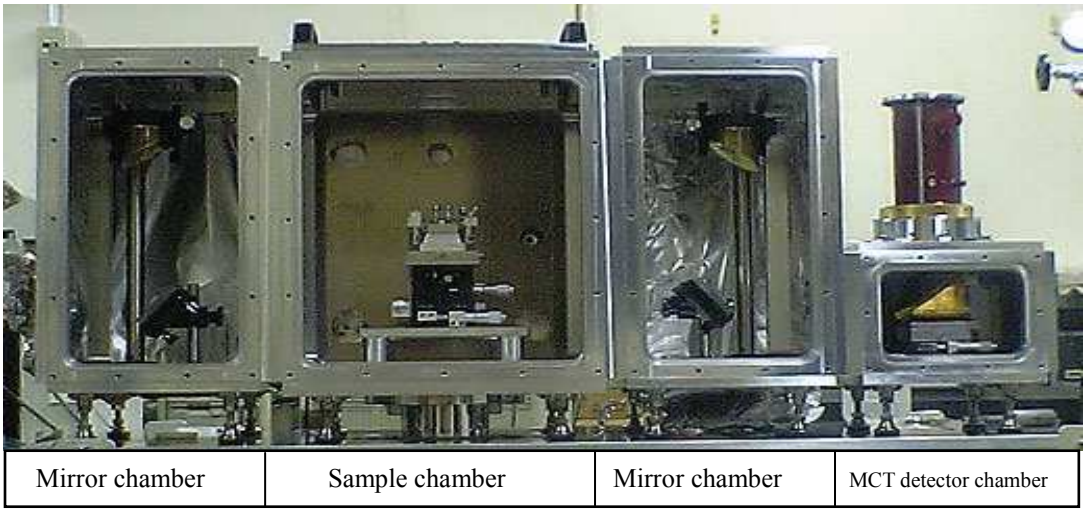

Figure 3.5 Picture of the NG-IRRAS sample chamber system

Figure 3.4 shows the schematic diagram of the sample chamber system for the new NG-IRRAS system. IR beam from the spectrometer is irradiated on an Al-coated plane mirror (M_1 in Figure 3.4) and reflected to an off-axis Au-coated paraboloidal mirror (M_2). These two mirrors guide the IR beam to the CaF_2 prism side plane to introduce the IR beam to the substrate surface with the angle of 64˚. The reflected IR beam from the substrate surface was focused onto the mercury cadmium telluride (MCT) detector using the mirrors M_3, M_4 and M_5. The MCT detector was cooled by liquid nitrogen. The mirror M_4 is an Al-coated plane mirror; M_3 and M_5 are off-axis Au-coated paraboloidal mirrors with diverting angle of 65° and 90° respectively. The sample chamber is sealed by two CaF_2 windows (V_1 and V_2 in Figure 3.4) with 5 mm thickness and 50 mm diameter. These CaF_2 view ports were used without coating. The picture of the sample chamber system is shown in Figure 3.5.

This new NG-IRRAS system can be used to detect biomaterials at the solid-solution interface as well as in vacuum, if the IR beam path and the sample chamber were arranged differently for each system, as shown in Figure 3.4b and 3.4c. A specified

sample holder was designed for each measurement. The detail of each sample holder is shown in Figure 3.6.

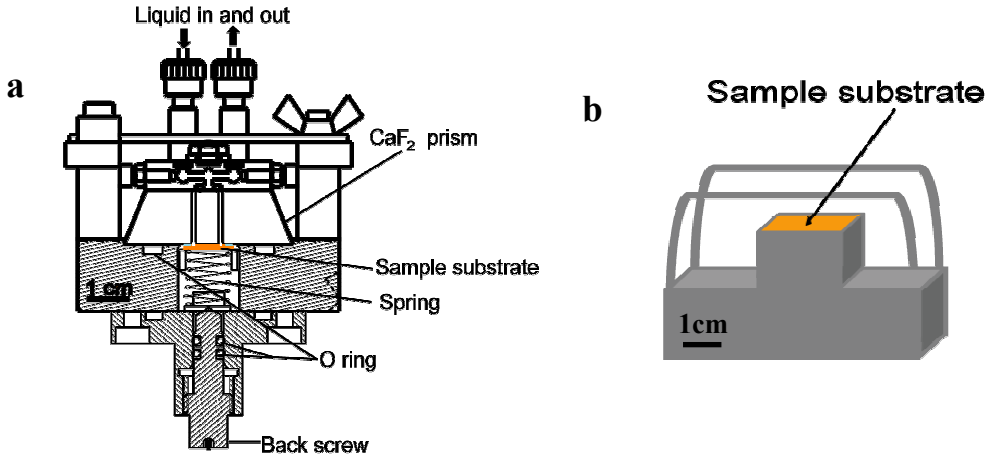

Figure 3.6 Detailed structures of sample holders; a) for the solid-solution interface NG-IRRAS, and b) for the vacuum IRRAS arrangement.

A CaF_2 prism (40×40×15) mm^3 was used in this NG-IRRAS system. For the IR measurement at the solid-solution interface, two through holes (diameter 2 mm) are made in the CaF_2 prism, to flow solutions in and out of the sample holder (shown in Figure 3.2). The solution is injected through Teflon tubes (inner diameter 0.5 mm) using a syringe pump connected to the solution inlet and outlet ports. The sample solution is injected by the syringe pump at a prescribed flow rate. The picture of the sample holder for solid-solution interface and the solution injection system are shown in Figure 3.7. For the vacuum IRRAS arrangement a simple metal block sample holder (Figure 3.6b) was used. A UV lamp was placed above on the substrate for ashing of the biomaterials. A UV lamp holder, electric connection to the UV lamp and dry air flow system was equipped in the IR sample chamber.

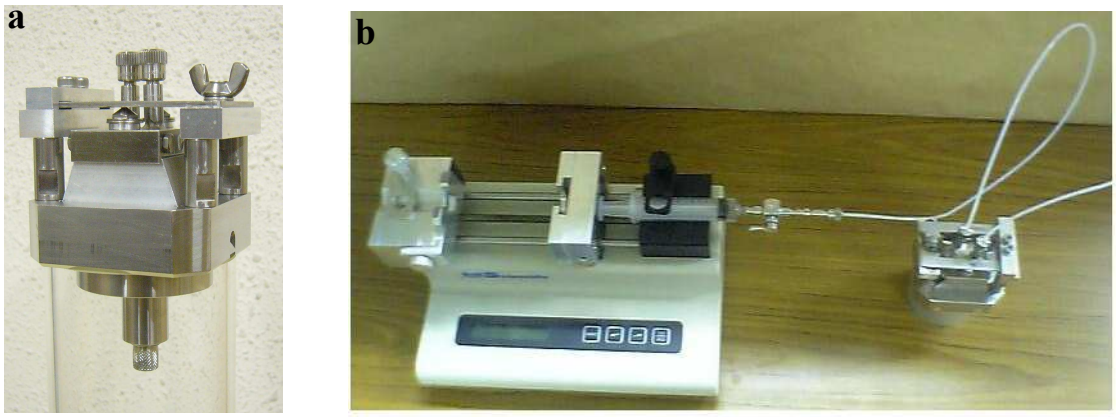

Figure 3.7 a) Picture of the sample holder for solid-solution interface biomaterials, drawn in Figure 3.6a. b) Picture of the solution injection system connected to the sample holder.

This NG-IRRAS system is available for any IR reflecting metal substrates. The size of sample substrate was 14×14×0.6 mm^3. In this study, two different substrates, the silicon substrate with a buried metal layer (BML) fabricated by the wafer-bonding method [17], and a commercial gold substrate were used to detect solid-solution interface biomaterials. An 8 μm thick nickel sheet (Nilaco Co.) of size 14×14 mm^2 with a 10×4 mm^2 rectangular window in the middle position was inserted between the sample substrate and the CaF_2 prism as a spacer, as shown in Figure 3.8. The sample substrate with the Ni spacer on its surface was placed on the movable sample stage, and then the CaF_2 prism was put upon the Ni spacer surface, finally the prism was combined with the solution supply system and locked with a screw. A spring (spring constant 6 N/mm) is used to push the movable sample stage as well as the sample substrate from the backside. The back screw was deigned to compress the spring. In this work, 2.5 mm compression of spring was used, and I investigated the tolerable solution thickness change (ΔLs; see section 5.3.2), the thickness change due to the injection pressure during the solution injection (ΔLp) and recovery of thickness change after stopping the injection (ΔLr) (Figure 3.8), which are expressed as

$$|\Delta Lp| - |\Delta Lr| < \Delta Ls$$

The back screw is sealed by two O-rings to minimize the gap change due to the looseness of the screw.

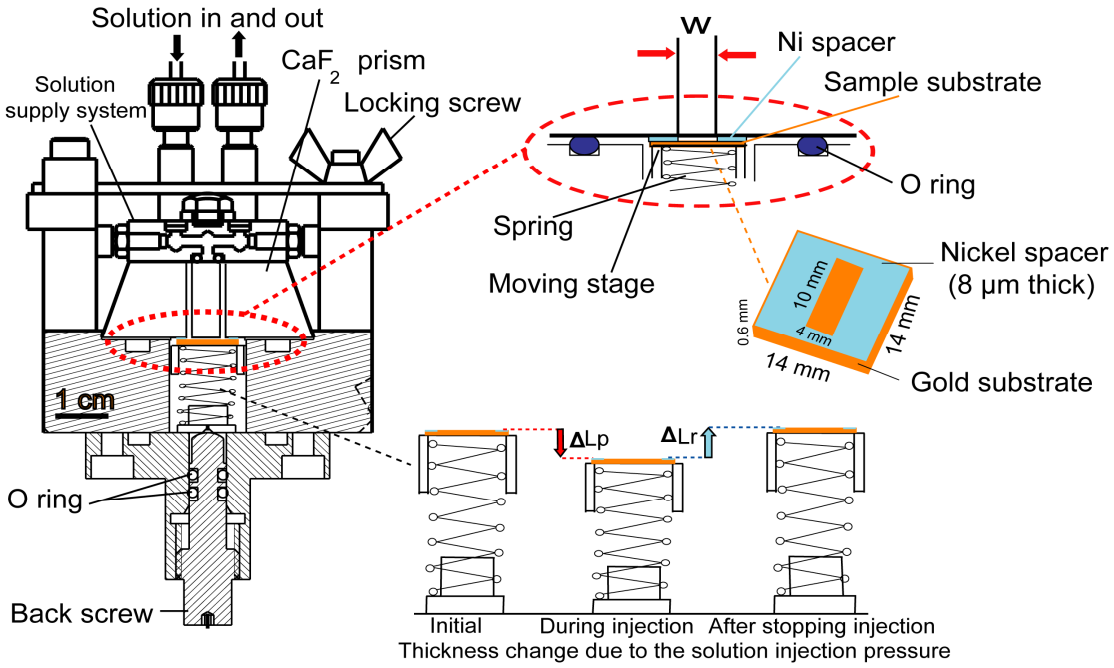

Figure 3.8 The schematic of the detailed set-up of the sample holder; solution thickness change due to the injection pressure, sample substrate and Ni spacer.

In this present NG-IRRAS system, the sample chamber is evacuated by a rotary pump (RP) and a turbo molecular pump (TMP) with 500 L/s pumping speed (Figure 3.3). The sample chamber was evacuated to minimize water vapor noise spikes from the IR spectra. Since the TMP is attached directly to the sample chamber, the TMP is turned off and the chamber is evacuated only by the RP during IRRAS measurements to avoid the influence of vibration. The vacuum condition was monitored by a Pirani gauge (ULVAC GP2A) and an ion gauge (ULVAC G1-M2). The base pressure was always kept less than 2×10^{-2} Torr.

3.3 Rearrangement of NG-IRRAS system to vacuum IRRAS

The NG-IRRAS system can be rearranged to vacuum IRRAS measurement. The sample chamber arrangement was shown in Figure 3.4c. In the IR measurement at the solid-solution interface, the IR light is refracted by the CaF_2 prism (Figure 3.9, solid yellow line), but in the vacuum IRRAS measurement the IR light directly illuminates on

the sample surface without refraction (Figure 3.9, dotted red line). Thus, the sample height should be adjusted to compensate the difference in the light path length.

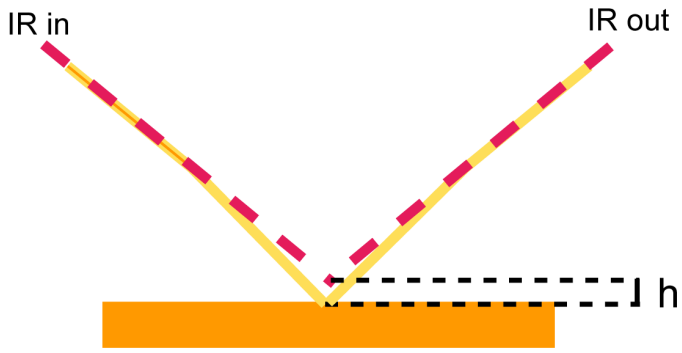

Figure 3.9 Sample height difference between the IRRAS measurement in vacuum and at the solid-solution interface. Yellow solid line represents the IR path for the solid-solution interface and the red dotted line for the vacuum IRRAS.

The IR reflection point without prism was evaluated to be ~2 mm higher, and the higher sample holder was made for the vacuum measurement. This sample holder (Figure 3.6b) was made of a steel block, and the sample substrate was fixed upon the holder using silicone grease.

3.4 Technical problems of the new NG-IRRAS system

The IR light passes through the water layer between the prism and the sample surface in this NG-IRRAS system. Thus, it is necessary to keep the water layer thickness constant to obtain a flat baseline. In this IRRAS system a special sample holder was used to control the water layer thickness in nanometer level fluctuations (Figure 3.6a, 3.7 and 3.8). Several factors were identified for the change of the water layer thickness in several nanometers. These factors and the resolution of them were described briefly in chapter 5.

3.5 Summary

A new NG-IRRAS system was constructed using a JEOL JIR-7000 FT-IR spectrometer and a home built sample chamber system. A sample holder using a CaF_2 prism was designed for observing adsorbed biomaterials at the solid-solution interface. The solution layer was kept at a prescribed thickness (usually 8 μm) by inserting a Ni spacer between the CaF_2 prism bottom and the substrate surface. To make the gap constant precisely, the sample substrate was pushed by a specially designed spring and O ring system from backside. The sample chamber was evacuated to remove water vapor from the IR spectra. Therefore, the sample solution was sealed with O-rings, and was injected through the holes in the CaF_2 prism at a prescribed speed using a syringe pump. The same optical setup was also used for a vacuum IRRAS. For vacuum IRRAS measurement a simple metal block sample holder was used, where the sample substrate was fixed by silicone grease on the metal block.

References

[1] D. L. Allara, J. D. Swallen, J. Phys. Chem. 86 (1982) 2700.

[2] D. F. Cui, V. A. Howarth, M. C. Petty, Thin Solid Films 192 (1990) 391.

[3] Z. Liu, M. D. Amiridis, Surf. Sci. 596 (2005) 117.

[4] N. Misawa, S. Yamamura, Y.-H. Kim, R. Tero, Y. Nonogaki, T. Urisu, Chem. Phys. Lett. 419 (2006) 86.

[5] A. Kerth, A. Erbe, M. Dathe, A. Blume, Biophys. J. 86 (2004) 3750.

[6] C. W. Meuse, S. Krueger, C. F. Majkrzak, J. A. Dura, J. Fu, J. T. Connor, A. L. Plant, Biophys. J. 74 (1998) 1388.

[7] C.R. Flach, J. W. Brauner, J. W. Taylor, R. C. Baldwin, R. Mendelsohn, Biophys. J. 67 (1994) 402

[8] A. Meister, C. Nicolini, H. Waldmann, J. Kuhlmann, A. Kerth, R. Winter, A. Blume, Biophys. J. 91 (2006) 1388

[9] L. Wang, P. Cai, .H-J Galla, H. He, C. R. Flach, R. Mendelsohn, Eur. Biophys. J. 34 (2005) 243.

[10] P. Cai, C. R. Flach, R. Mendelsohn, Biochemistry 42 (2003) 9446.

[11] J. W. Brauner, C. R. Flach, Z. Xu, X. Bi, R. N. A. H. Lewis, R. N. McElhaney, A. Gericke, R. Mendelsohn, J. Phys. Chem. B 107 (2003) 7202.

[12] D. L. Elmore, R. A. Dluhy, Appl. Spectrosc. 54 (2000) 956.

[13] K. K. Chittur, Biomaterials 19 (1998) 357.

[14] S. Morita, M. Tanaka, Y. Ozaki, Langmuir 23 (2007) 3750.

[15] D. D. Popenoe, S.M. Stole, M. Porter, Appl. Spectrosc. 46 (1992) 79.

[16] H. Seki, K. Kunimatsu, W.G. Golden, Appl. Spectrosc. 39 (1985) 437.

[17] S. Yamamura, S. Yamuchi, S. Watanabe, M. Tabe, T. Kasai, Y. Nonogaki, T. Urisu, Jpn. J. Appl. Phys. 42, (2003) 3942.

Chapter 4

Experimental: details with materials and methods

(Chem. Phys. Lett. 466 (2008) 235.)

4.1 Sample substrate cleaning

In the newly developed narrow gap solid-solution infrared reflection adsorption spectroscopy (NG-IRRAS) system, adsorbed fibronectin (FN) and immunoglobulin G (IgG) were investigated at the interface between aqueous solutions and SiO_2 or gold surfaces. The substrates were cleaned before using in sample investigation. Two different methods were followed for cleaning these substrates. All the following processes were performed in a clean room.

4.1.1 Cleaning of BML-substrate

A Si wafer with a buried metal layer (BML) fabricated by the wafer-bonding method [1], which have the structure of SiO_2(100)/$CoSi_2$/ Si (100), was RCA-cleaned as follows. Firstly, the BML substrate was sonicated in acetone and methanol, each for five minutes, to remove oil and grease from the substrate. Afterward the BML substrate was boiled in piranha solution (conc. H_2SO_4 + H_2O_2 (30%) (4:1 v/v)) (to remove organic compounds and metal contamination) and then in NH_4OH (20%) + H_2O_2 (30%) + H_2O (1:4:20 v/v) (to remove particles) for 10 minutes each. Then the BML substrate was immersed in 1% HF solution to remove native SiO_2 resulting in a hydrophobic H-terminated Si surface.

Finally, the substrate was boiled in a mixed solution of HCl and H_2O_2 (conc. HCl + H_2O_2 (30%) + H_2O (1:1:4 v/v)) (to oxidize the metal surface). Then the substrate was kept in miliQ (>18 MΩ cm^{-1}) water until the use in experiments. Through this protocol a quite flat (rms roughness of 0.18 nm) chemically oxidized SiO_2 layer is formed on the BML substrate.

4.1.2 Cleaning of gold substrate

The gold substrate, which was formed by depositing gold on a Cr-coated glass substrate (*Au/ Cr / glass)*, was purchased from Moritex Co. (Tokyo, Japan). In this work, the as-delivered gold substrate was immersed in acetone and methanol and the beaker was agitated with hand for two minutes, each. Then the gold substrate was washed with miliQ water and dried with N_2 blow. The dried gold substrate was placed in a glass beaker carefully keeping gold side up. Then 7.5 mL 30% H_2O_2 was poured onto the gold substrate and subsequently 15 mL conc. H_2SO_4 was added into the glass beaker. This solution, i.e. piranha solution, was mixed gently. The gold substrate was kept in the piranha solution for 2 h with being gently agitated for every 15 minutes interval. Then the piranha solution was slowly decanted to the other beaker. MiliQ water was poured onto the gold substrate to wash out the piranha solution. The miliQ water was exchanged at least 10 times to completely remove the piranha solution from the gold substrate. Finally, the gold substrate was dried with gentle N_2 flow and kept in a box until the IgG deposition.

4.2 Materials and sample preparation

FN from human plasma was purchased from Sigma-Aldrich Inc. (St. Louis, MO). The FN vial was first equilibrated to RT and dissolved in D_2O (Sigma-Aldrich) for at least 30 min at the concentration of 5 mg/ml. The FN solution was stored in working aliquots (100 μL) at -20ºC. The FN solution was taken out from the refrigerator, kept at RT, and warmed in a water bath at 37°C for ~ 20 min, before it was injected into the IRRAS sample holder.

Purified mouse IgG was purchased from Sigma-Aldrich (St. Louis, MO) and used without further purification. The stock solution of IgG (5 mg/mL) was prepared using 0.85% NaCl solution of D_2O as the solvent and kept at – 20°C in 75 µL aliquot. The IgG aliquot was re-warmed to RT and injected into the IRRAS sample holder.

2-methoxy-(polyethylene) oxypropyltrimethoxysilane (PEG) (Gelest, PA) was dissolved in HPLC grade ethanol (Wako Pure Chemical Industries Ltd., Japan) at the concentration of 5% (v/v). H_2O was removed from 10 mL H_2O-phosphate buffered saline (PBS) (pH 7.4) (Wako) by evaporation and again dissolved to 10 mL D_2O, to prepare D_2O-based PBS solution. 16-mercaptohexadecanoic acid (MHA) (Sigma-Aldrich) was used to prepare self assembled monolayers (SAM) on gold surface. N-(3-dimethylaminopropyl)-N'-ethylcarbodiimide hydrochloride (EDC) and N-hydroxysuccinimide (NHS) (Sigma-Aldrich) were used to active the MHA-SAM on the gold surface. D_2O solution of 0.4 M EDC and 0.1 M NHS solutions were preserved in working aliquots at -20^{o}C.

4.3 Prism surface cleaning and PEG coating on prism bottom surface

In this experiment, a trapezoidal CaF_2 prism with two through holes was used to flow solutions in and out of the sample holder. It was necessary to clean every time. The smooth CaF_2 prism bottom surface was rinsed by flowing ~ 50 mL of chloroform and immersed in acetone and ethanol at RT for 10 min and 30 min, respectively. Finally the surface was rinsed with water, dried with N_2 blow, and kept in a vacuum for 10 min.

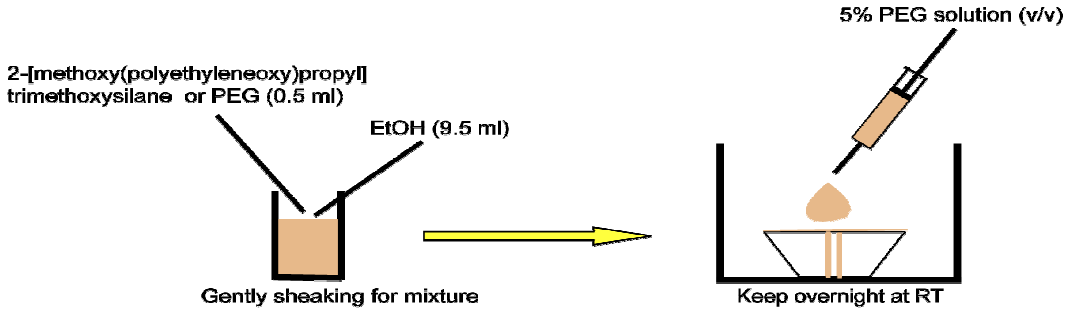

Figure 4.1 The schematic protocol of PEG coating on the CaF_2 prism surface.

Since PEG coating was reported to prevent the non-specific protein adsorption on solid surfaces [2, 3], PEG coating was deposited on the CaF_2 prism surface. The prism bottom was fully covered with a freshly prepared 5% PEG solution (4 - 5 mL) and settled still for 4 h, then the same amount of PEG solution was added on the same surface and left overnight. The excess PEG solution on the prism surface was removed by dipping the prism in ethanol and MiliQ water, and then the prism was dried with N_2 blow and kept in a vacuum for 10 min, before it was set in the NG-IRRAS sample holder. The protocol of PEG coating on the CaF_2 prism surface is shown in Figure 4.1.

4.4 Preparation and activation of MHA-SAM on gold surface

SAMs of various thiols with different structures have been investigated on gold surfaces [4]. Thiols are used due to their spontaneous chemisorptions, regular organization and high thermal, mechanical and chemical stability on gold surfaces [5]. Long chain thiols and sulfides have been shown to be more thermally stable [6] and the adsorption to the surface has been shown to proceed by two processes [7], (1) ionic dissociation and more favorably by (2) radical formation.

$$RSH + Au \longrightarrow RSAu^{-} + H^{+} \text{.....(1)}$$

$$RSH + Au \longrightarrow RSAu^{\cdot} + H^{\cdot} \text{.....(2)}$$

Preparation protocol of binary SAM of MHA and 3-mercaptopropionic acid (MPA) on gold surface has been reported by Yu et al. [8]. In the report the gold surface was immersed in MHA mixture solution. In my experiment, the piranha-cleaned gold substrate was washed with ethanol in a beaker, and immersed in a 10 mM ethanol solution of MHA for 24 h at RT. The substrate surface was taken out from the MHA solution and washed with ethanol and miliQ water. The SAM-coated gold surface (-COOH terminated) was kept in miliQ water until it was used.

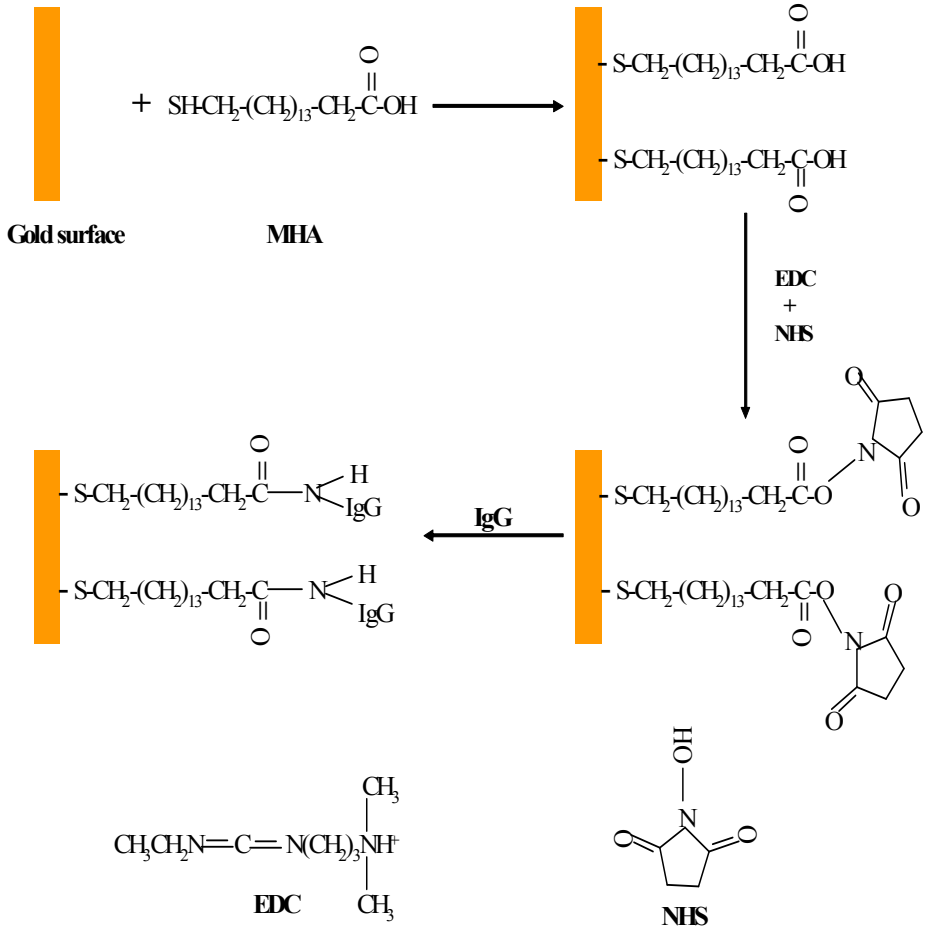

Figure 4.2 Immobilization of IgG on the gold surface via an activated MHA-SAM.

The –COOH terminated MHA-SAM surface was activated for the peptide-bond formation with the $–NH_2$ group of IgG surface, using a 1:1 (v/v) mixture of 0.4 M EDC and 0.1 M NHS. Just before the activation of the MHA-SAM, EDC and NHS solution were thawed at RT and the same volume of 0.4 M EDC and 0.1 M NHS solutions were mixed. Then, 200 µL of EDC and NHS mixture solution was dropped on the SAM coated

gold substrate and kept for 10 min at RT. Then the activated MHA-SAM surface was washed with PBS buffer and placed in the NG-IRRAS sample holder. The immobilization of IgG on this activated surface is described in the next section

4.5 Immobilization of FN and IgG

FN is often used as an extra cellular matrix in the cell culture on SiO_2 substrates [9]. Therefore, FN was chosen for the in-situ observation at the interface between the BML substrate and solution using new NG-IRRAS system. The FN solution (5 mg/mL, 100 μL) was injected in the sample holder, and remained for 3 h to adsorb on the SiO_2 surface of BML substrate.

It has been reported that IgG easily adsorbs on hydrophobic, hydrophilic and modified surfaces [10, 11]. The adsorption state on three different surfaces, non-coated gold, MHA-SAM and activated MHA-SAM was investigated by the new NG-IRRAS system. Warmed IgG aliquot was injected and remained 1 h for non-coated and MHA-SAM coated surface and 30 min for activated MHA-SAM coated surface. Immobilization protocol of IgG on the activated MHA-SAM surface is shown in Figure 4.2. The covalent bond forms between –COOH of the SAM and $–NH_2$ of lysine residues, which are distribute almost homogeneously on the IgG surface [12].

References

[1] S. Yamamura, S. Yamuchi, S. Watanabe, M. Tabe, T. Kasai, Y. Nonogaki, T. Urisu, Jpn. J. Appl. Phys. 42, (2003) 3942.

[2] N. Xia, Y. Hu, D.W. Grainger, D.G. Castner, Langmuir 18 (2002) 3255.

[3] K. Uchida, H. Otsuka, M. Kaneko, K. Kataoka, Y. Nagasaki, Anal. Chem. 77 (2005) 1075.

[4] R. D. Vaughan, C. K. O'Sullivan, G. G. Guilbault, Fresenius J. Anal. Chem. 364 (1999) 54.

[5] M. Ohtani, T. Sunagawa, S. Kuwabata, H. Yoneyama, J. Electroanal. Chem. 396

(1995) 97.
[6] C. D Bain, E. B. Troughton, Y. T. Tao, J. Evall, G. M. Whitesides, R. G. Nuzzo, J. Am. Chem. Soc. 111 (1989) 321.
[7] H. M. Schessle, D. S. Karpovich, G. J. Blanchard, J. Am. Chem. Soc. 118 (1996) 9645.
[8] C. Yu, A. Ganjoo, H. Jain, C.G. Pantano, J. Irudayara, J. Anal.Chem. 78 (2006) 2500.
[9] T. Urisu, T. Asano, Z.-L. Zhang, H. Uno, R. Tero, H. Junkyu, I. Hiroko, Y. Arima, H. Iwata, K. Shibasaki, M. Tominaga, Anal Bioanal Chem. 391 (2008) 2703
[10] C. E. Giacomelli, M.G. E. G. Bremer, W. Norde, J. Colloid Interface Sci. 220 (1999) 13.
[11] J. Buijs, W. Norde, Langmuir 12 (1996) 1605.
[12] N. Misawa, S.Yamamura, Y.-H. Kim, R. Tero, Y. Nonogaki, T. Urisu, Chem. Phys. Lett. 419 (2006) 86.

Chapter 5

Origins of baseline distortions and their removal

(Chem. Phys. Lett. 466 (2008) 235.)

5.1 Introduction

It is the most difficult and important problem to realize the stable and flat baselines in the NG-IRRAS measurement of solid-solution interface. The IR absorbance of the bulk solution layer is affected by any changes of the solution layer thickness [1], resulting in the baseline distortion. In the new NG-IRRAS system a special sample holder (Figure 3.6, 3.7 and 3.8 in section 3) was used to control the gap thickness in nanometer level between the CaF_2 prism surface and sample surface during the injection of reagent solution. But the distorted baseline spectra were found, even if the special sample holder was used. Several technical problems were identified for the baseline fluctuations, which are explained in this chapter. In the following chapter, spectra were taken at 2×10^{-2} Torr with 20 scanning accumulation with a spectral resolution of 4 cm^{-1} as Happ-Genzel function.

5.2 The characteristic of IR power spectra of the NG-IRRAS system

CaF_2 is transparent for IR light in the range of 1250-4200 cm^{-1}. Therefore, in the NG-IRRAS, this wavenumber region can be used to observe the vibrational modes of biomolecules. Since the noise increases in proportion to the inverse of the IR intensity, I first measured the IR power spectra after passing through the sample holder under several conditions. At the condition where IR beam s introduced to the CaF_2 prism bottom

surface with the total reflection condition, the whole IR region (1250-4000 cm^{-1}) was highly transparent and the observed power spectrum is shown in Fig. 5.1 A. A Si substrate with buried-metal-layer (BML) [2] was used as a substrate to measure the power spectrum when the gap is filled with D_2O or H_2O, as shown in Figure 5.1 B, and C, respectively.

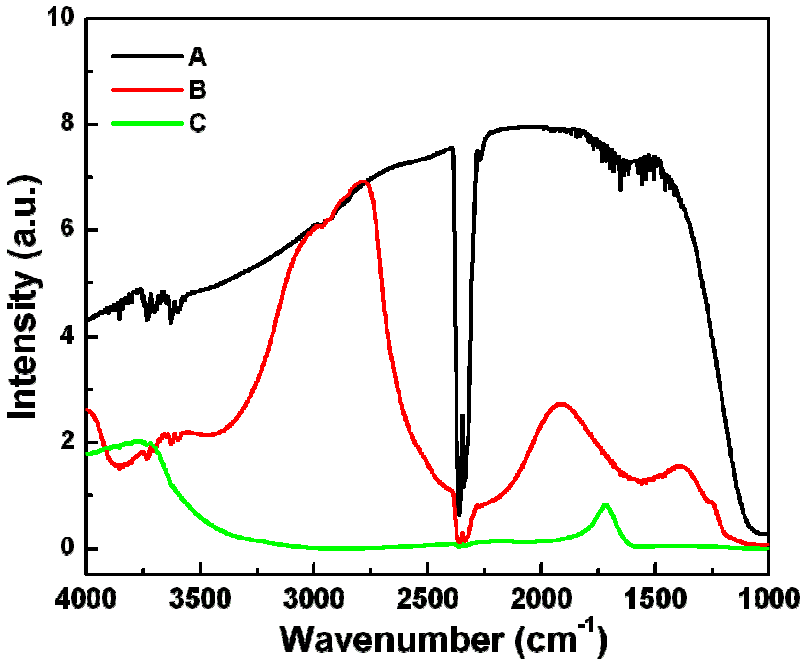

Figure 5.1 The IRRAS power spectra measured by the NG-IRRAS system A) The power spectrum of the beam reflected at the CaF_2/air interface by the total internal refection condition. The power spectrum of the beam which reflected at the BML substrate surface when 8 μm thick B) D_2O or C) H_2O layer exists between the CaF_2 prism and BML substrate.

The IR light is almost absorbed by the H_2O layer at the region of 1000-3750 cm^{-1}(Figure 5.1 spectrum C), while the D_2O layer gives higher intensity at almost the whole region (1250-4000 cm^{-1}) especially in the region of 2700-3100 cm^{-1} (Figure 5.1 spectrum B). Thus, it is clear from the IR power spectra (Figure 5.1) that H_2O is not suitable for the in-situ observation of adsorbed biomaterials at the solid-solution interface.

5.3 Baseline characteristics

In the attenuated total internal reflection (ATR-IR) technique, the effective water layer thickness is automatically prefixed by the penetration depth of the IR beam at the ATR crystal-water interface [3, 4]. On the other hand, in NG-IRRAS system the IR light passes through the water layer between the prism and the sample surface [5, 6]. So, the change in the water layer thickness affects baseline absorbance. Previous repots showed that the absorbance of full-coverage protein is ~ 5×10^{-3} [7, 8]. I assumed the required condition of the baseline fluctuation to be Δ abs. $<10^{-3}$, thus the tolerance of the solution thickness changes (ΔLs) is evaluated ~ 4 nm using $\alpha = 2.6 \times 10^{3}$ (absorbance coefficient of water at 1600 cm^{-1}).

I have developed a special sample holder and equipped a syringe pump to control the water layer thickness during the injection of reagent solution with nanometer level fluctuation. Variation of sample holder temperature, injection flow speed and bubbles in water are also the key factors for the change of the water layer thickness.

5.3.1 Thermal effects on solution layer thickness

The 8 μm thick Ni sheet (Nilaco Co.) was used as a spacer to keep the water layer thickness constant. The base line fluctuation due to the thermal effect can be calculated by considering the thermal expansion of the spacer as follows.

$$I = I_o \exp(-\alpha L) \qquad (1)$$

$$\text{Abs.} = -\log(I/I_o)$$

$$= \alpha L, \qquad (2)$$

Where, I_o and I are incident and transmitted IR beam power, respectively, and α = absorption coefficient, L = thickness of the solution layer (μm), and Abs. is the absorbance.

Considering the condition in the absorbance fluctuation, ΔAbs. $< 10^{-3}$,

then,

$$\alpha \ \Delta L < 10^{-3} \qquad (3)$$

$$\alpha = (4\pi/\lambda)\, k \qquad (4)$$

$$(4\pi/\lambda)\, k \ L\, \theta\, \Delta T < 10^{-3}, \qquad (5)$$

where, k = extinction coefficient of D_2O (The extinction coefficient of D_2O is approximated from the less vibrational region of H_2O around 2000 cm^{-1}, the estimated k (D_2O,1600 cm^{-1}) = ~ 0.01 (Appendix III)), θ = thermal expansion coefficient of Ni, ΔL = variation of the solution layer thickness, ΔT= temperature change (°C) and λ = wavelength (cm^{-1}).

In the present NG-IRRAS, Ni was chosen for its low thermal expansion coefficient and also for its non-corrosive nature to the solution. The thermal expansion coefficient of Ni is 1.33 x 10^{-5} (K^{-1}) and those of other different metals are shown in appendix IV. The absorbance change at 1600 cm^{-1} at which the amide I band, the important absorption region of proteins, is observed, due to the thermal expansion of the Ni spacer is calculated to be ~0.3 $\times 10^{-5}$ per degree centigrade. The room temperature fluctuation is sufficiently controlled less than 1 K. The temperature fluctuation of the prism due to the absorption of IR beam was also measured using the thermo couple to be sufficiently less than 1 °C. So, I concluded that the base line fluctuation due to the thermal effect is ignorable in the present NG-IRRAS system.

5.3.2 Injection flow speed effects on the solution layer thickness

To observe reactions at the solid-solution interface using NG-IRRAS, a solution injection system to control the injection speed was equipped with the system as described in section 3.2. The gap between the CaF_2 prism and the substrate surface was settled at 8 μm by using the Ni spacer. Water pressure depends on the injection flow, which is applied by a syringe pump during the injection of the reagent solution into the gap. I calculated the pressure difference of the solution (ΔP) between the inlet and the outlet of the solution layer approximately by using the following equation,

$$\Delta P = \frac{32\mu u l}{D^2}$$

u= speed of D_2O (m/s)
μ= viscosity of D_2O (Ns/m^2)
l= length of the path (m)
D=diameter of the path (m)

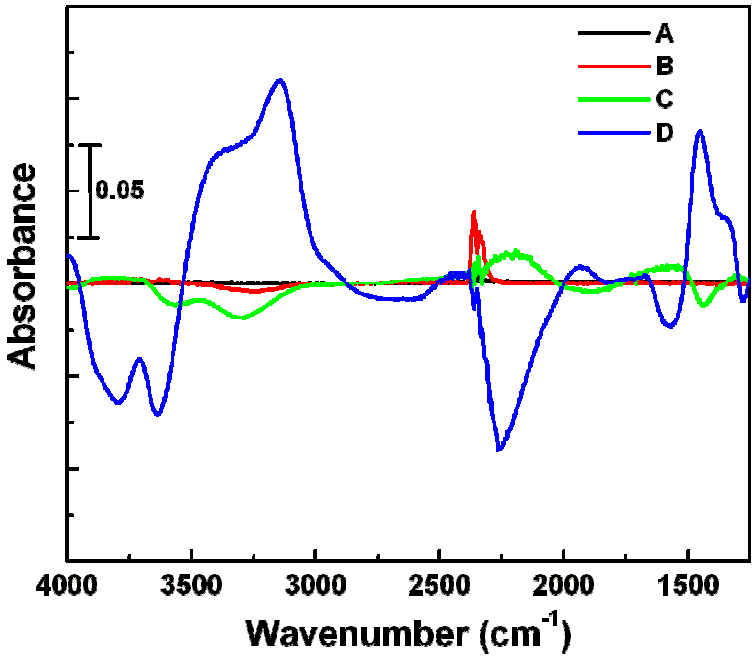

Figure 5.2 Baseline fluctuations due to the injection flow speed. The baselines are measured with the injection rates of (A) 2, (B) 5, (C) 10, and (D) 30 mL/h.

Using the following parameter values, the area of the sample solution layer (S) = (4 x 10^{-3} m) x (10 x 10^{-3} m), the cross section of the sample solution layer (A) = (8 x 10^{-6} m) x (4 x 10^{-3} m), μ = 1 x 10^{-3} (N s/m^2), and assuming D^2 = 4/3.14 x A, I obtained the pressure difference (ΔP) value of ~ 70 N/m^2 for 1 mL/h injection speed. A spring (spring constant 6 N/mm) is used to press the sample stage from the backside in the present system. Considering the atmospheric pressure at solution outlet, I assumed that the half of the pressure ~ 35 N/m^2 is applied to the sample stage by the pressure from the syringe pump, and the thickness change of the sample solution layer by this pressure (ΔLp) was calculated to be ~ 245 nm. After the injection is stopped, the pressure of the solution from the sample stage is eliminated and the spring at the backside of the sample substrate pushes back to the original position (recovery of thickness change after stopping the injection (ΔLr), section 3.2, Figure 3.8). But the gap width does not recover precisely to the original position if the injection pressure is large, and significantly distorted baseline

appears (Figure 5.2). I have investigated the optimum injection flow speed and found that at maximum 2 mL/h flow speed is tolerable for this NG-IRRAS sample holder. The gap change is suppressed within the required level for the adsorbed protein layer (ΔLs = ~ 4 nm) when the injection speed is kept <2 mL/h. Larger injection speed than 2 mL/h caused serious baseline distortion as shown in Figure 5.2. Therefore, I have decided the maximum injection speed to be 2 mL/h.

5.3.3 Base line fluctuation due to air bubble in injected solutions

If any air bubble is included in the solution between the CaF_2 prism and sample surface, total internal reflection of the IR light occurs at the CaF_2/ air bubble interface. The reflectivity of the IR light changes depending on the position and size of the bubble, which is unpredictable. Several examples of the air bubble effects on the baseline spectra is shown in Figure 5.3. Before the injection of reagent solutions, I confirmed visually that there was no air bubbles in the solution.

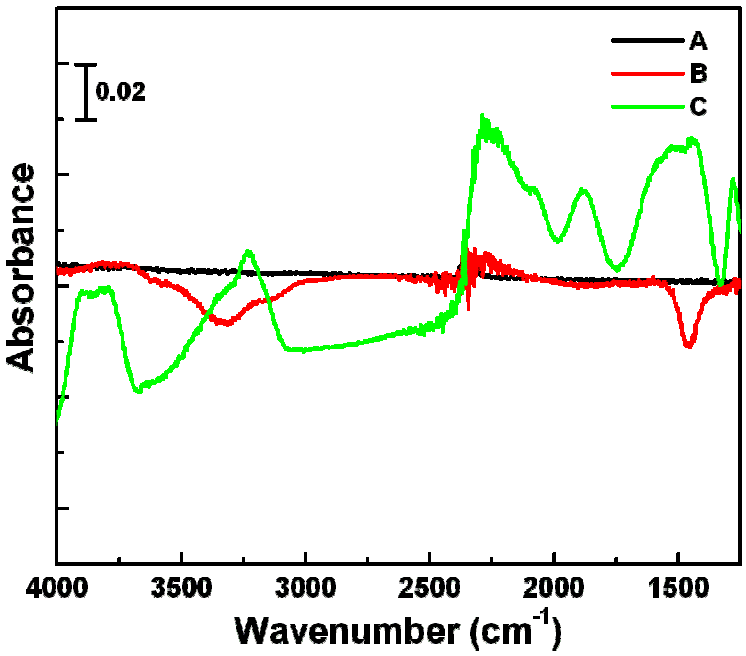

Figure 5.3 Examples of baseline fluctuations due to the air bubbles in the solution. The baselines are measured (A) without air bubble, and (B, C) with bubbles in the independent experiments.

5.3.4 Baseline fluctuations due to the adsorbed water on optical systems

In the NG-IRRAS, the spectrum was taken in vacuum condition of the sample chamber to avoid water vapor effects on the baseline. All the spectra were taken at ~2×10^{-2} Torr. The dependence of the baseline spectrum on the evacuation time was shown in Figure 5.4. This fluctuation of the baseline is due to the changes of the adsorbed amount of water on the prism and the IR view ports of the system during the measurements.

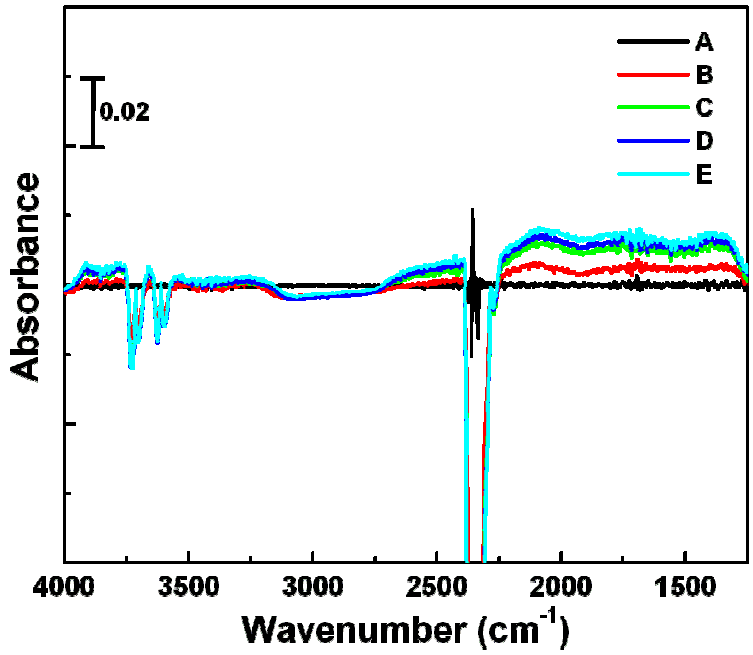

Figure 5.4 The baseline taken after different evacuation time. (A) 2 (B) 3 (C) 4 (D) 5, and (E) 6 h.

The distortion of the baseline was gradually eliminated with the increase of evacuation time. Figure 5.5 shows the spectra of baselines taken after 6 h or longer evacuations. From figures 5.4 and 5.5, it is found that evacuation of 6 h is necessary for this NG-IRRAS system to remove water vapor effects from the baseline.

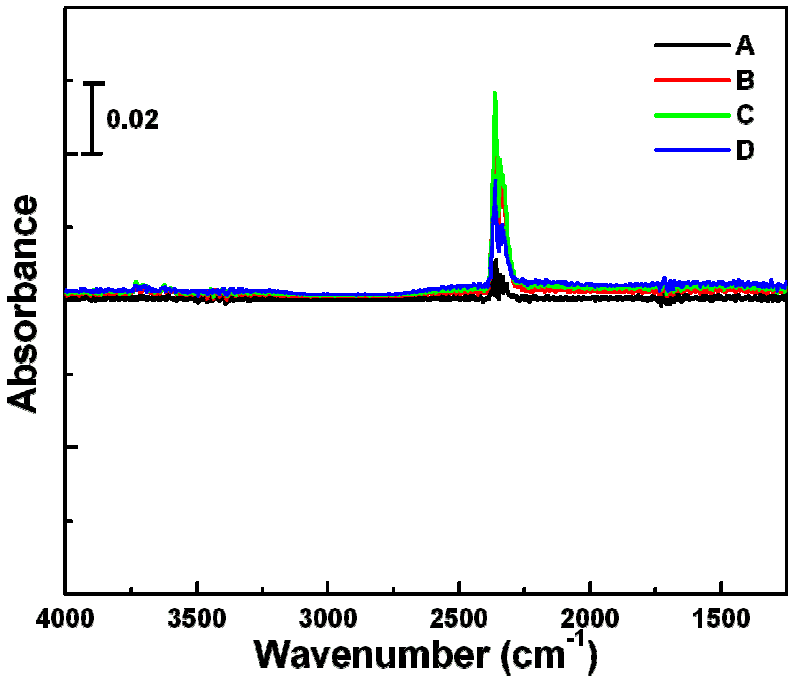

Figure 5.5 (A) The baseline after 6-h vacuum pumping. (B) 30 min (C) 1 h, and (D) 2 h longer evacuation than (A).

From these experiments in this chapter, I have concluded that the conditions for the flat and stable baselines are i) minimum 6 h evacuation of sample chamber, ii) injection speed less then 2 mL/h, iii) room temperature fluctuation within 1 K, and iv) a 8 μm thick Ni spacer with a slit of 4 mm×10 mm.

References

[1] M. Osawa, Bull. Chem. Soc. Jpn. 70 (1997) 2861.

[2] S. Yamamura, S. Yamuchi, S. Watanabe, M. Tabe, T. Kasai, Y. Nonogaki, T. Urisu, Jpn. J. Appl. Phys. 42, (2003) 3942.

[3] K.K. Chittur, Biomaterials 19 (1998) 357.

[4] R. A. Dluhy, S. M. Stephens, S.i Widayati, A. D. Williams, Spectrochimica Acta Part A 51 (1995) 1413-1447

[5] D.D. Popenoe, S.M. Stole, M. Porter, App. Spectrosc. 46 (1992) 79.

[6] H. Seki, K. Kunimatsu, W.G. Golden, App. Spectrosc. 39 (1985) 437.

[7] N. Misawa, S. Yamamura, Y.-H. Kim, R. Tero, Y. Nonogaki, T. Urisu, Chem. Phys. Lett. 419 (2006) 86.

[8] M. J. Swamy, T. Heimburg, D. Marsh, Biophys. J. 71 (1996) 840.

Chapter 6

Application of new NG-IRRAS system for observation of solid-solution interface biomaterials

Chem. Phys. Lett. 466 (2008) 235.

6.1 Abstract

Based on the preliminary experiments written in the previous chapter, I have constructed a new system of narrow gap infrared reflection absorption spectroscopy (NG-IRRAS) for solid-solution interface biomaterials. A sample solution is confined in a narrow space between the CaF_2 prism and the substrate surface. The sample holder is specially designed to keep the narrow space constant during the measurement process. Absorption spectra of immunoglobulin G (IgG) in the solution phase and at the interface between the solution and carboxyl-terminated self assembled monolayer on the gold surface with and without covalent bonding have been clearly observed with good reproducibility. Noticeable molecular conformation change induced by the adsorption was not observed.

6.2 Introduction

Infrared reflection absorption spectroscopy (IRRAS) is an attractive technique for studying biomaterials on solid surfaces. This technique has been applied to IR non-transparent solid surfaces [1-4] or to the air-solution interfaces [5-8], where the attenuated total reflection (ATR) technique [9] cannot be applied. Biosensors such as surface plasmon resonance (SPR) [10,11] and quartz crystal microbalance (QCM) [12, 13], which are now widely used to detect biomaterials such as DNA and many kinds of pathogenic markers, are important for obtaining information and increasing measurement reliability of molecular structures with biomaterials adsorbed on the substrate surface.

Measuring the IR spectrum of the adsorbed biomaterials on their substrates is considered a promising method for solving this problem. At present, however, a conventional IR measurement method, which can be simply applied to these biosensor substrates, does not exist. A narrow gap IRRAS (NG-IRRAS) with a prism/narrow solution layer/substrate arrangement [14, 15], to which these biosensor substrates can be directly attached from the substrate side, may potentially fulfill this requirement. In the NG-IRRAS reported up to now, however, the solution layer is too thin (1~2 μm) for monitoring chemical reactions, and it is not easy to increase this layer thickness and inject solutions. A thick solution layer causes a significantly large noise of the baseline due to its strong IR absorption. Injections of a reagent solution into the narrow solution layer easily change the solution layer thickness, which causes a significant distortion of the baseline. There is also another problem in NG-IRRAS. Measurement must be conducted under the condition that the sample biomaterial is not adsorbed on the prism surface.

Thus, to develop a new NG-IRRAS method that can be applied for characterization of the solid-solution interface adsorbates on biosensor substrates, I must solve the following two technical problems: (1) to keep the narrow solution layer thickness constant within nanometer-level variations during observations including the reagent and washing solution injection processes, and (2) to establish that the sample materials are adsorbed on the substrate surface but not on the prism surface. Since IRRAS is sensitive to

submonolayer adsorbates, several nanometers-level variation of the solution layer thickness causes significant fluctuation of the baseline, even if using D_2O solution. The adsorption of sample materials on the prism surface also significantly disturbs the absorption spectrum of the sample materials on the substrate surface. I believe that the reason why there are no reported applications of NG-IRRAS to the monitoring of chemical reactions is the difficulty in solving these two problems. Concerning the adsorption of proteins on the solid surfaces, it is important to apply suitable coating to make the surface inert for adsorption [16-20] and to control both surface charges and salt effects of proteins [21, 22], by which the aggregation followed by precipitation is induced .

I have developed an in-situ NG-IRRAS instrument for monitoring chemical reactions and characterizations of the solid-solution interface adsorbates on the IR-nontransparent substrates. The sample holder is specially designed so that the solution layer thickness between the CaF_2 prism surface and the substrate surface is kept constant during measurement and the prism surface is coated with PEG (2-methoxy-(polyethylene) oxypropyltrimethoxysilane) for resisting adsorption of biomaterials [18, 20]. To show the usefulness of the developed NG-IRRAS instrument, I have demonstrated the measurement of the amide I band of immunoglobulin G (IgG) at the interface between the solution and the self-assembled-monolayer (SAM)-coated gold surface. No noticeable molecular conformation change of IgG is found to be induced by covalent bonding to the SAM on the gold substrate.

6.3 New NG-IRRAS system

6.3.1 Design of IRRAS measurement system

JIR-7000 FT-IR spectrometer (JEOL Ltd., Japan) was used as an IR light source in this system. Non-polarized IR light was directly illuminated to the prism edge of the sample holder, and the IR beam reflected on the substrate surface was focused onto the detection area of the mercury cadmium telluride (MCT) detector cooled with liquid nitrogen. A schematic of the IRRAS system is shown in Figure 3.4a (chapter 3). Only the p-

polarization is active at the solid-solution interface in IRRAS; therefore, no polarizers were used. The interferometer housing and the IR optics system were purged with dry air. A rotary pump (RP) and a turbo-molecular pump (TMP) evacuate the sample chamber at 500 L/s. The TMP was stopped and the chamber was pumped only by the RP during the IRRAS measurement to avoid the effects of vibration, because the TMP was attached directly to the sample chamber. The vacuum was monitored using a Pirani gauge (GP2A, ULVAC Inc., Japan) and an ion gauge (G1-M2, ULVAC). The base pressure was always kept below 2×10^{-2} Torr. Two different sample holders were used in this system for measuring biomaterials on a solid surface under solution (Figure. 3.4b) and in a vacuum system (Figure. 3.4c).

6.3.2 Sample holders

A number of factors were considered in the designing of the sample holder for the NG-IRRAS system. The water layer was kept to a prescribed thickness (usually 8 μm) by inserting a Ni spacer between the CaF_2 prism bottom and the substrate surface. The gap remained constant during the injection of the solution by pushing the substrate from the back with a 2.5-mm-compressed spring with a spring constant of 6N/mm, and a screw with an O-ring seal was deigned so that the back lash was minimized (Figure 3.8). The sample chamber was evacuated to remove water vapor. The sample solution was sealed with O-rings, as shown in Figure 3.8, and was injected with a syringe pump at a prescribed flow speed. The same optical setup was also used for a vacuum IRRAS, as shown in Figure 3.6b, where the sample substrate was fixed onto a metal block.

6.3.3 UV ashing

To measure the spectrum under a vacuum, the substrate was placed on the sample holder and fixed with silicone grease. A UV lamp was placed ~ 2 cm above the substrate surface (Figure 3.4c). The sample chamber was filled with dry air during UV-ashing. The IR spectra of signal (S) and background (B) are obtained in a vacuum before and after UV-ashing, respectively, and the absorbance was obtained by $-\log(S/B)$.

6.4 Materials

6.4.1 Sample preparation

FN and IgG (Sigma-Aldrich) stock solutions (5 mg/mL) were prepared using D_2O (Sigma-Aldrich) and 0.85% NaCl solution of D_2O, respectively, without further purification and kept at –20 °C in 100-µL (FN) and 75-µL (IgG) aliquot. The FN solution was taken out from a refrigerator 1 h before the measurement of IRRAS and kept at room temperature (RT), and warmed for ~ 20 min in a water bath at 37 °C. Finally, it was injected into the IRRAS sample holder. The IgG aliquot was re-warmed to RT before use, and injected into the IRRAS sample holder. A 5% PEG (Gelest, PA) (v/v) solution was prepared using HPLC grade ethanol (Wako Pure Chemical Industries Ltd., Japan). 10 mL phosphate buffered saline (PBS)/H_2O (pH 7.4) (Wako) was evaporated and again dissolved to 10 mL D_2O, to prepare D_2O-based PBS solution.

6.4.2 Treatment of the substrate surface

IRRAS is applicable only to reflective metal surfaces. Therefore, I used a buried-metal-layer (BML) substrate, which has a structure of SiO_2 (100)/$CoSi_2$/Si (100) formed by wafer-bonding method [23], since FN is often used as an extra cellular matrix in the cell culture on SiO_2 substrates [24]. The BML substrate was RCA-cleaned by successive treatment with the following solutions: conc. H_2SO_4 + H_2O_2 (30%) (4:1 v/v), NH_4OH (20%) + H_2O_2 (30%) + H_2O (1:4:20 v/v), HF solution (1%), and conc. HCl + H_2O_2 (30%) + H_2O (1:1:4 v/v).

The gold substrate, which was formed by depositing Cr (a few nanometers thick) and Au (45 nm thick) on a (14 × 14 mm^2) glass substrate, was purchased from Moritex Co. (Tokyo, Japan). The as-delivered gold substrate was used after cleaning with piranha solution [25], and it was not reused. The cleaned surface was coated with a SAM, which was formed by dipping the gold substrate into a 10-mM ethanol solution of 16-mercaptohexadecanoic acid (MHA) (Sigma-Aldrich) for 24 h at RT and washing with MilliQ water. This MHA-SAM coated surface is terminated with –COOH. IgG physisorption and covalent chemisorption on this hydrophilic surface was examined by

the NG-IRRAS. For the chemisorption through covalent bonding, this –COOH terminated surface was activated with a 1:1 v/v mixture of 0.4-M N-(3-dimethylaminopropyl)-N'-ethylcarbodiimide hydrochloride (EDC, Sigma-Aldrich) and 0.1-M N-hydroxysuccinimide (NHS, Sigma-Aldrich).

6.4.3. Treatment of the prism surface

The CaF_2 prism-bottom surface was coated with PEG as follows. The highly smooth CaF_2 prism-bottom surface was rinsed with ~ 50 mL of chloroform. Then the surface was immersed in acetone and ethanol for 10 and 30 min, respectively, at RT. Finally the surface was rinsed with water, dried with N_2 blow, and kept in a vacuum for 10 min. The prism bottom was fully covered with freshly prepared 5% PEG solution (4 ~ 5 mL) and settled still for 4 h, then the same amount of PEG solution was added on the same surface and left overnight. Finally, excess PEG solution on the prism surface was removed by dipping in ethanol and MilliQ water, and the prism was dried with N_2 blow and kept in a vacuum for 10 min.

6.5. IRRAS measurement

6.5.1. Baseline characteristics

For solid-solution interface IRRAS measurements, the sample holder shown in Figure 3.8 was used. A several nanometers-level change in the gap between the prism and the substrate surfaces caused a significant fluctuation of the baseline spectrum due to IR absorption by the solution. The injection flow speed of the sample solution, which caused the fluctuation of the gap, should be carefully controlled. In the present system, the baseline was sufficiently flat so long as the injection speed was kept below 2 mL/h, as shown in Figure 6.1. The RT fluctuation was controlled to less than 1 °C. This sufficiently suppressed the noise from gap fluctuation by thermal expansion to less than 10^{-4} absorbance. The noise from the adsorbed water on the optical component surface was also reduced sufficiently after a long (6 h) evacuation of the sample chamber. The baseline characteristics obtained after all these careful operations are shown in Figure 6.1. The baseline is sufficiently flat in the wide range of 1250 - 4000 cm^{-1}. Even after a 6 h pumping, an insignificant time dependent drift of the baseline, due to the slight

adsorption of water on the CaF_2 window and prism surfaces was observed (section 5.3.4, Figure 5.3 and 5.4).

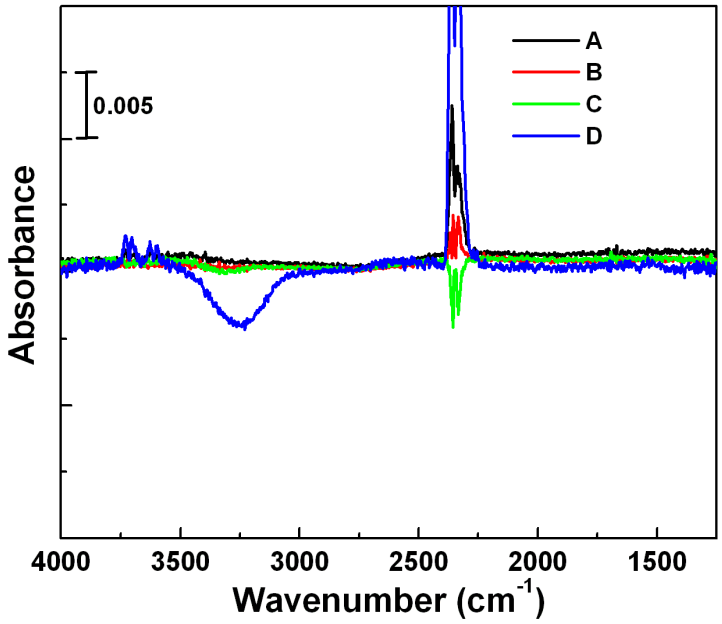

Figure 6.1 Dependence of baseline after 6-h vacuum pumping on the injection rate. The baselines are measured with injection rates of (A) 0.5, (B) 1.0, (C) 2.0, and (D) 5.0 mL/h.

6.5.2. Protocol of the IRRAS measurements

The IRRAS spectrum was measured using the following protocol.

1. Set up the sample holder system (Figure 6.1a) using the CaF_2 prism, the Ni spacer, and the gold or BML substrate.
2. Evacuate the chamber for 1 h.
3. Take a FTIR spectrum, which is the background spectrum (B_p) for the prism surface adsorbate, and then the sample chamber, was leaked to air.
4. Inject the D_2O solution at 2 mL/h. Here, four kinds of D_2O solution were used; pure D_2O, NaCl (140 mM) D_2O solution, D_2O-based PBS solution, and NaCl-added (140 mM) D_2O-based PBS solution.

5. Evacuate the chamber for 6 h.
6. Take the FTIR spectrum, which is the background spectrum (B_s) for the samples in the solution phase and the adsorbate on the substrate surface.
7. Inject 100 μL of FN or 75 μL of IgG D_2O solution (5 mg/mL) at a rate of 2 mL/h and leave it for 3 h (FN), 1 h (IgG on non-activated SAM surface) or 0.5 h (IgG on activated surface).
8. Take the signal spectrum (S_1). Remove the sample solution with an injection of 0.5 mL of pure D_2O or D_2O-based solutions, and take the signal spectrum S_2. Repeat this operation 4 more times and take the signal spectrum, S_3, S_4, S_5, and S_6 in each operation.
9. Disassemble the sample holder, wash the prism and the substrate surface gently with 1 mL D_2O, and gently dry the prism and substrate surface with N_2 blow. Then set up the sample holder again and evacuate for 1 h. Keep the substrate at 4°C under a vacuum.
10. Take the spectrum, which is the signal spectrum (S_p) for the prism surface adsorbate.
11. Change the sample holder to vacuum type (Figure 6.1b) and paste the dried substrate (from the protocol 9) with silicone grease.
12. Take the spectrum of the adsorbate on the substrate under a vacuum (S_v).
13. Remove the adsorbate from the substrate surface using UV ashing.
14. Take the background spectrum of the substrate surface without adsorbate under a vacuum (B_v).
15. Absorbance spectrum for each case is obtained by calculating – log (S_i/B_j) for corresponding S_i and B_j.

All spectra were recorded with a 400-scan accumulation with a spectral resolution of 4 cm^{-1} as a Happ-Genzel function.

6.6 Control of the salt effects

As mentioned above, specific adsorption of proteins on desired solid surfaces is an important issue in bio-chips and bio-sensors. Many ideas for preventing nonspecific adsorption on surfaces have been reported. For example, surface modification using PEG-tethered chains leads to a significant reduction in the nonspecific interaction of biological molecules [17, 19]. Other than the surface coating, control of pH and the effects of salt [21, 22] prevent the precipitation or aggregation of dissolved biomolecules and minimize the non-specific adsorption of proteins on the surface.

Since all CaF_2 [26], SiO_2 [24, 27], and gold [11, 16-18, 20] surfaces are active in protein adsorption, I have investigated the inert condition of the solution for FN and IgG adsorption on the PEG-coated CaF_2 prism surface. I found that the conditions were completely different in these two proteins. Figure 6.2a shows the adsorption of FN on the PEG-coated prism surface depending on the solution condition. The absorbance spectra obtained by $-\log(S_p/B_p)$, where S_p and B_p are defined in Section 6.5.2, shows the amide I band with a peak around 1630 cm^{-1}. It is clear that significant adsorption on the prism surface occurs with the PEG-coated surface when D_2O-based PBS solution is used (line A in Figure 6.2a). On the other hand, an almost insignificant amount of FN is observed on the PEG-coated surface (line B in Figure 6.2a) under pure D_2O.

IgG significantly adsorbs on the PEG-coated prism surface when pure D_2O is used as a solvent, as shown in Figure 6.2b. The adsorption of IgG on the prism surface significantly declines when a NaCl solution of ~140 mM or higher is used. The adsorption tendency on the prism surface is the completely opposite with salt concentrations between FN and IgG.

Here, I consider the significant difference between FN and IgG in the adsorption characteristics on the PEG-coated prism surface. The isoelectric points of FN and IgG are 5.5 - 6.3 [28-31] and 6.5 - 9.5, respectively [32]. Since the pH of the solutions was 7.4 in these experiments, the FN molecules are negatively charged in the pure D_2O solution, and aggregation followed by precipitation is hindered by intermolecular coulomb repulsion. In the PBS solution, on the other hand, the electrical double layer becomes

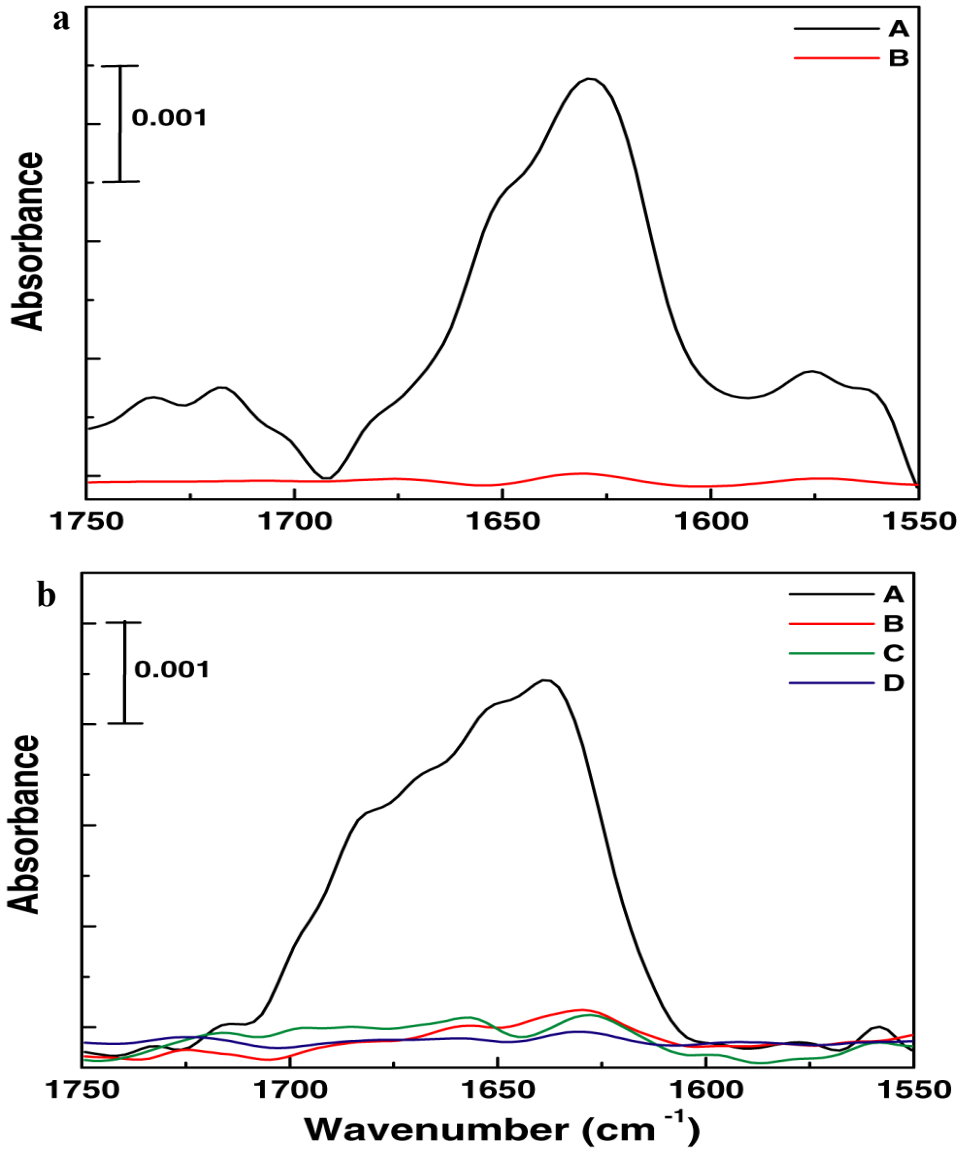

Figure 6.2 Amide I bands of adsorbed proteins on a PEG-coated prism surface measured with the total internal reflection (TIR) arrangement (protocols 3 and 10 in Section. 4). a) Spectra of FN using (A) D_2O-based PBS solution, and (B) pure D_2O as solvents. b) Spectra of IgG using (A) pure D_2O, (B) NaCl (140 mM) D_2O solution, (C) D_2O-based PBS solution and (D) NaCl-added (140 mM) D_2O-based PBS solution as solvents.

very thin (less than ~ 0.82 nm) and enhances attractive intermolecular interaction due to the van der Waals force. Therefore, significant aggregations of FN followed by adsorption on the prism surface are induced.

IgG is almost neutral in pure D_2O, and coulomb repulsion does not work. Furthermore, since no electric double layer exists in pure D_2O, attractive and repulsive forces between the intra-molecular positive and negative charges strongly interact with each other, resulting in the deformation of IgG molecular conformation. In an IgG molecule, more than 50% of the inside hydrophobic β-sheet conformation is covered by α-helix, turn, and random coil conformations on the surface [33]. In D_2O, the hydrophobic area located at the inner position of the protein molecule is possibly exposed by the deformation of molecules due to the strong intramolecular coulomb interaction, resulting in the aggregation of IgG on the prism surface. For salt solutions, such as PBS, NaCl (140 mM), or mixtures of them, the coulomb interaction between the intra-molecular charges almost completely disappears and the IgG molecule keeps the natural structure stable. Thus, I believe that the salt effects governing the formation of the electrical double layer explain the observed significant difference between FN and IgG with adsorption characteristics on the prism surface.

6.7 IRRAS measurement of FN on BML surface

FN was observed at D_2O/BML interface, the first IRRAS was taken 3 h after the FN injection into the narrow gap between the prism and BML Surface (Figure 6.3 a-A). Then the IRRAS spectra were repeatedly taken after every 0.5 mL D_2O flushes at 2 mL/h. The spectrum A in Figure 6.3a contains the signal from both FN dissolved in D_2O and adsorbed on the substrate surface. The spectrum F was taken after 2.5 ml D_2O flushing, which is mainly from the FN adsorbed on the BML surface. The amide I band of FN was observed at approximately 1637 cm^{-1} (β sheet) with shoulders around 1671 and 1683 cm^{-1} (β turn) [34]. The IRRAS spectrum of FN adsorbed on the BML substrate surface was also measured in the vacuum condition. The amide I band of FN was significantly different from that in the solution, as shown in Figure 6.3b. This change of amide I band

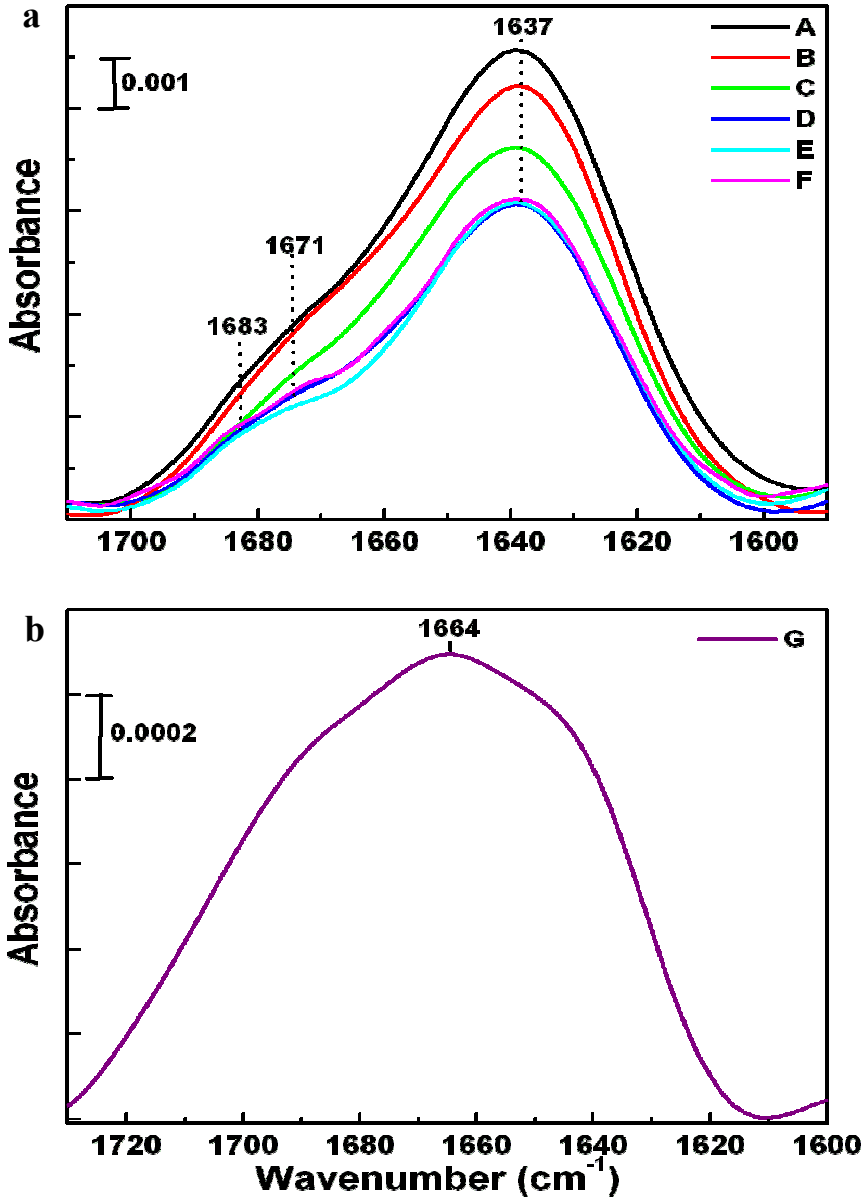

Figure 6.3 a) The amide I bands of adsorbed FN on BML substrate surface under D_2O solution measured using protocols 6, 7, and 8 in Section 6.5.2. Spectra A to F are $\log (S_i/B_s)$ with $i = 1$ to 6, respectively.
b) Spectra of adsorbed FN on the BML substrate measured in a vacuum.

is due to the denaturation of the proteins during the removal of water from the substrate surface.

6.8 IRRAS measurement of IgG on SAM-coated gold surfaces

IgG molecules are widely used for various immunochemical and biochemical analyses. Thus the molecular conformation of IgG at the solid-solution interface is an important issue of the assay performance. The amount of the structural components in IgG fragments, determined using X-ray diffraction [35, 36], are 45 and 47% of β-sheets and 7 and 2% of α-helices for the Fc and Fab segments of IgG, respectively. It should be noted that these data are taken in its solid state and that no interactions with solvents are involved. The IR spectrum of IgG solution is discussed by Gorga et al. [33] using the transmission arrangement. In their work, however, adsorption of IgG on the inner surface of the sample holder was not evaluated. The adsorption-induced conformation change is an important topic of IgG, and it was reported that adsorption on a hydrophobic surface enhances the formation of α-helices and random coils, while the β-sheet content is reduced [27].

I measured the IRRAS of IgG physisorbed and covalently bonded on MHA-SAM-coated gold surfaces and investigated the adsorption-induced conformation change. After activation of the MHA-SAM surface using the EDC and NHS mixture solution, the substrate was attached to the sample holder, NaCl-added (140 mM) D_2O-based PBS solution of IgG was injected, and IRRAS was measured according to the protocol described in Section 6.5.2. Similar IRRAS spectra were obtained for IgG adsorbed on a hydrophilic non-activated SAM-coated surface (Figure 6.4a). Spectra A to F in Figure 6.4a show the observed amide I bands with IgG covalently bonded to the activated SAM surface, corresponding to S_1 to S_6, respectively, in Section 6.5.2. The absorptions in Figure 6.4a correspond to the previously reported secondary structure ratio of IgG: 64% β-sheet (1639 cm^{-1}), 28% turns (1672 and 1683 cm^{-1}) and minor α-helix component (1657 cm-1) [33]. Figure 6.4a shows that the intensity of the amide I band decreases with every 0.5-mL washing, and the band shape becomes almost constant after ~ 1.5 mL of washing.

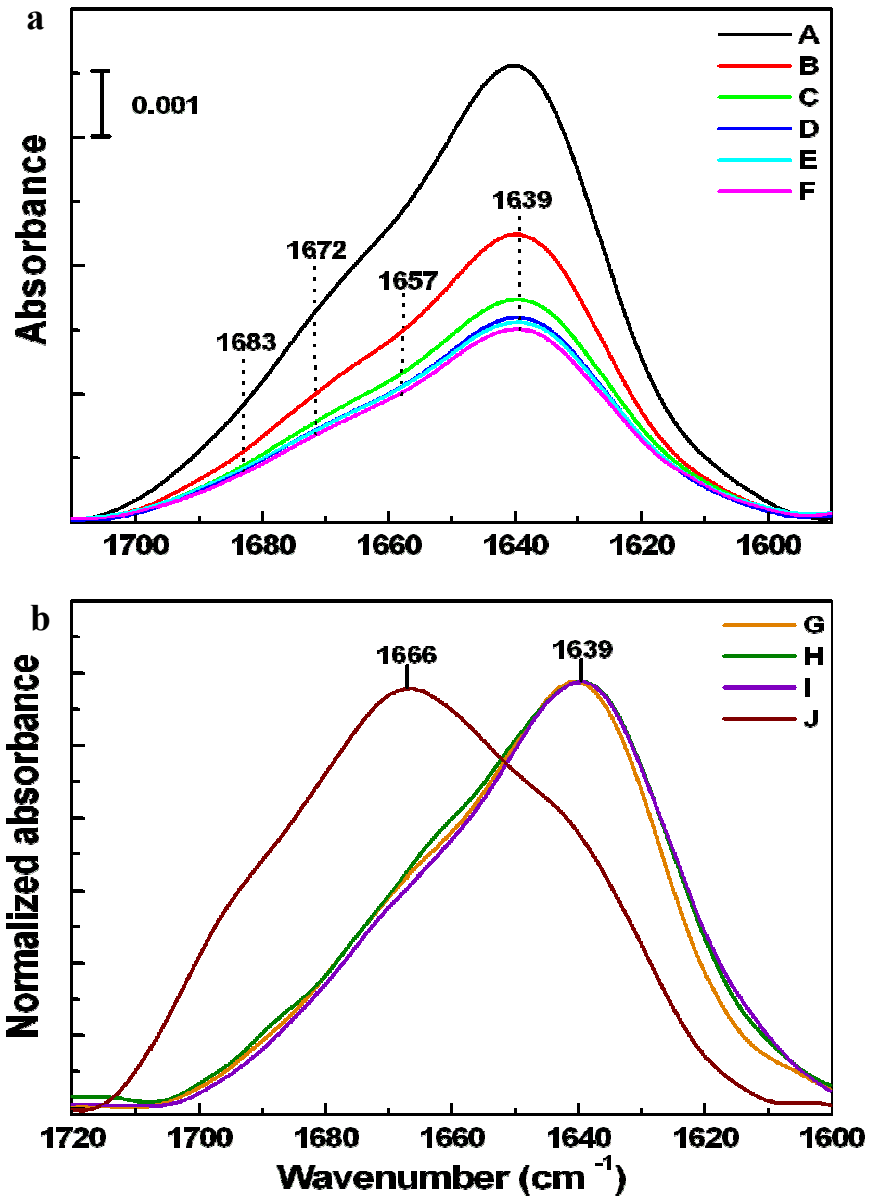

Figure 6.4 a) The amide I bands of adsorbed IgG on activated SAM-coated gold substrate surfaces under NaCl-added (140 mM) D_2O-based PBS solution measured using protocols 6, 7, and 8 in Section 4. Spectra A to F are $\log (S_i/B_s)$ with $i = 1$ to 6, respectively.

b) Spectra of IgG (G) dissolved in the solution, (H) adsorbed on the non-activated MHA-SAM under the solution, (I) adsorbed on the activated MHA-SAM under the solution, and (J) adsorbed on the activated MHA-SAM measured in a vacuum.

This means that the observed band after 1.5 mL of washing is assigned to the absorption due to the adsorbed (solid-solution interface) IgG molecules, and the bands before the 1.5-mL washing is the sum of the absorptions due to solution phase and solid-solution interface IgG. Therefore, the solution phase spectrum can be obtained from the spectral difference between A and D (or E or F) for NG-IRRAS, as shown in Figure 6.4a. The amide I bands for adsorbed IgG at the solid-solution interface on the activated and non-activated MHA-SAM surfaces are shown as spectra I and H in Figure 6.4b, respectively, and spectrum G in Figure 6.4b is the IgG in the solution. The amide I band of IgG molecules adsorbed on the activated SAM surface was also measured under a vacuum ($-\log S_v/B_v$), as shown in Figure 6.4b (spectrum J). Significant denature due to the removal of water from the substrate surface was observed. On the other hand, in the case of IgG without water removal (spectra G-I in Figure 6.4b), no clear difference in the shape of amide I band of IgG was observed between the solution state and the covalently bonded state on the activated SAM surface, other than a peak shift of ~ 1 cm^{-1}. This clearly indicates that no noticeable molecular conformation change is induced by the covalent bonding on the activated SAM surface. I suppose that the molecular orientation of adsorbed IgG is random since lysine residues, which form covalent bonding with –COOH on the SAM surface [4], are distributed almost homogeneously on the IgG surface. Similarly, no clear adsorption-induced deformation was observed in the absorption spectrum of IgG adsorbed on the non-activated (hydrophilic) MHA-SAM surface (Figure 6.4b, H), which agrees with the reported result [37].

6.9 Summary

I have constructed a new NG-IRRAS system, which is applicable for solid-solution interface biomaterials adsorbed on metal or BML substrate surfaces at submonolayer sensitivity. This system confines the sample solutions in a narrow (~ 8 μm) gap between a CaF_2 prism and a substrate surface. The sample holder was specially designed so that the gap remains constant during the injection of the solution within a certain injection speed. Adsorption of proteins on the prism surface, which interferes with precise measurement, was suppressed using PEG-coating of the prism surface and controlling the solution pH

and the effects of the salt. The amide I bands of the IgG molecules dissolved in the solution and covalently bonded to the COOH-terminated SAM surface have been clearly recorded for the first time. No noticeable indication of the conformational change of IgG induced by the covalent bonding to the SAM surface on the gold substrate has been observed.

References

[1] D.L. Allara, J.D. Swallen, J. Phys. Chem. 86 (1982) 2700.

[2] D. Malevich, J. Li, M. K. Chung, C. McLaughlin, M. Schlaf, J. Lipkowski, J. Solid State Electrochem. 9 (2005) 267.

[3] Z. Liu, M.D. Amiridis, Surf. Sci. 596 (2005) 117.

[4] N. Misawa, S.Yamamura, Y.-H. Kim, R. Tero, Y. Nonogaki, T. Urisu, Chem. Phys. Lett. 419 (2006) 86.

[5] C. R. Flach, J.W. Brauner, J.W. Taylor, R.C. Baldwin, R. Mendelsohn, Biophys. J. 67 (1994) 402.

[6] C.R. Flach, Z. Xu, X. Bi, J. Brauner, R. Mendelsohn, Appl. Spectrosc. 55 (2001) 1060.

[7] A. Keith, A. Erbe, M. Dathe, A. Blume, Biophys. J. 86 (2004) 3750.

[8] A. Meister, C. Nicolini, H. Waldmann, J. Kuhlmann, A. Kerth, R. Winter, A. Blume, Biophys. J. 91 (2006) 1388.

[9] K.K. Chittur, Biomaterials 19 (1998) 357.

[10] R. Ziblat, V. Lirtsman, D. Davidov, B. Aroetiy, Biophys. J. 90 (2006) 2592.

[11] C. Yu, A. Ganjoo, H. Jain, C.G. Pantano, J. Irudayaraj, Anal. Chem. 78 (2006) 2500.

[12] J.H. Teichroeb, J.A. Forrest, L.W. Jones, J. Chan , K. Dalton, J. Colloid Interface Sci. 325 (2008) 157.

[13] R.J. Rawle, C.R.D. Selassie, M.S. Johal, Langmuir 23 (2007) 9563.

[14] D.D. Popenoe, S.M. Stole, M. Porter, App. Spectrosc. 46 (1992) 79.

[15] H. Seki, K. Kunimatsu, W.G. Golden, App. Spectrosc. 39 (1985) 437.

[16] C. Roberts, C.S. Chen, M. Mrksich, V. Martichonok, D.E. Ingber, G.M. Whitesides, J. Am. Chem. Soc. 120 (1998) 6548.

[17] R.E. Holmlin, X. Chen, R.G. Chapman, S. Takayama, G.M. Whitesides, Langmuir 17 (2001) 2841.

[18] N. Xia, Y. Hu, D.W. Grainger, D.G. Castner, Langmuir 18 (2002) 3255.

[19] M. Shen, M.S. Wagner, D.G. Castner, B.D. Ratner, T.A. Horbett, Langmuir 19 (2003) 1692.

[20] K. Uchida, H. Otsuka, M. Kaneko, K. Kataoka, Y. Nagasaki, Anal. Chem. 77 (2005)

1075.
[21] A.V. Dobrynin, R.H. Colby, M. Rubinstein, Macromolecules 28 (1995) 1859.
[22] A.C. Dumetz, A.M. Chockla, E.W. Kaler, A.M. Lenhoff, Biochim. Biophys. Acta 1784 (2008) 600.
[23] S. Yamamura, S. Yamuchi, S. Watanabe, M. Tabe, T. Kasai, Y. Nonogaki, T. Urisu, Jpn. J. Appl. Phys. 42 (2003) 3942.
[24] T. Urisu, T. Asano, Z.-L. Zhang, H. Uno, R. Tero, H. Junkyu, I. Hiroko, Y. Arima, H. Iwata, K. Shibasaki, M. Tominaga, Anal Bioanal Chem. 391 (2008) 2703.
[25] C.D. Bain, J. Evall, G.M. Whitesides, J. Am. Chem. Soc. 111 (1989) 7155.
[26] L. Dreesen, Y. Sartenaer, C. Humbert, A.A. Mani, J.-J. Lemaire, C. Méthivier, C.-M. Pradier, P.A. Thiry, A. Peremans, Thin Solid Films 464-465 (2004) 373.
[27] J. Buijs, W. Norde, Langmuir 12 (1996) 1605.
[28] J. Paul, R.O. Hynes, J. Biol. Chem. 259 (1984) 13477.
[29] M. Vuento, M. Wrann, E. Ruoslahti, FEBS Lett. 82 (1977) 227.
[30] H. Hörmann, Klin. Wochenschr. 60 (1982) 1265.
[31] J.W. Tamkun, R.O. Hynes, J. Biol. Chem. 258 (1983) 4641.
[32] F. Chiodi, Å. Sidén, E. Ösby, Electrophoresis 6 (1985) 124.
[33] J.C. Gorga, A. Dong, M.C. Manning, R.W. Woody, W.S. Caughey, J.L. Strominger, Proc. Natl. Acad. Sci. 86 (1989) 2321.
[34] S.-S. Cheng, K. K. Chittur, C. N. Sukenik, L. A. Culp, K. Lewandowska, J. Colloid Interface Sci. 162, (1994) 135.
[35] M. Marquart, J. Deisenhofer, R. Huber, W. Palm, J. Mol. Biol. 141 (1980) 369.
[36] R. J. Poljak, L.M. Amzel, B. L. Chen, R. P. Phizackerley, F. Saul, Proc. Natl. Acad. Sci. 71 (1974) 3440.
[37] C. E. Giacomelli, M.G. E. G. Bremer, W. Norde, J. Colloid Interface Sci. 220 (1999) 13.

Chapter 7

Summary

Several IR techniques, namely transmission infrared spectroscopy, infrared reflection absorption spectroscopy (IRRAS), and attenuated total reflection infrared spectroscopy (ATR-IR), have been widely used for the study of biomaterials. ATR-IR and IRRAS are available for studying adsorbates on solid surfaces. ATR-IR is a very effective technique for studying biological materials because the sample can be readily oriented on the ATR crystal and kept in an aqueous environment. But IR-non-transparent materials can not be used in the ATR-IR technique, which can be easily applicable in IRRAS. Therefore, for my doctoral course research, I have constructed a new narrow gap infrared reflection absorption spectroscopy (NG-IRRAS) system to observe biomaterials on IR-non-transparent metals at solid-solution interfaces.

This new NG-IRRAS system was constructed using a JEOL JIR-7000 FT-IR spectrometer and a home built sample chamber system. This NG-IRRAS system can be arranged to a vacuum IRRAS system. Two different sample holders, a specially designed and a simple metal block are use to observe biomaterials at solid-solution interface and in vacuum, respectively. The sample holder for the solid-solution interface was designed using a CaF_2 prism having two through holes for solution flow by a syringe pump. The water layer thickness was kept 8 μm by inserting a Ni sheet spacer between the CaF_2 prism bottom and the substrate surface. The gap remained constant during the injection of the solution by pushing the substrate from its back side with a 2.5-mm-compressed spring.

This NG-IRRAS is only applicable in D_2O based aqueous solutions because the IR

transmission is suppressed in H_2O at the almost whole effective wavenumber range. Specially designed sample holder was used to control the water layer thickness less than nanometer level for flat baseline. But temperature, solution flow rate, air bubbles in the solution and adsorbed water of the optical components were found as factors for the baseline distortion. I have investigated the suitable conditions to minimize all effects on the baseline spectrum. For a stable and flat baseline, the conditions such evacuation for at minimum 6 h; injection rate less then 2 mL/h and a Ni spacer thickness of 8 μm were necessary. The room temperature fluctuation was controlled within 1°C.

This NG-IRRAS system was used to investigate the protein adsorption at solid-solution interface. But, the adsorbed sample proteins were also found on the prism surface during the measurement, and were not distinguishable in the IRRAS spectra from signal of the proteins on the sample surface. 2-Methoxy-(polyethylene) oxypropyltrimethoxysilane (PEG) was coated on the CaF_2 prism surface to make the surface inert and resist non-specific adsorption of the protein on it. But, only the PEG coating was not enough for resisting the adsorption of proteins on CaF_2 prism surface. Thus, I have investigated the condition, in which the sample materials were adsorbed on the sample substrate surface but not on the PEG-coated prism surface. The adsorption of protein on PEG-coated prism surface was suppressed sufficiently by controlling the pH and salt effects of the solution, and appropriate conditions were different for each protein.

Fibronectin (FN) adsorptions on various surfaces have been extensively studied in several techniques such as atomic force microscopy (AFM) and ATR-IR. I have investigated the adsorbed FN at BML-solution interface using this NG-IRRAS. FN adsorbed on the PEG-coated prism surface in D_2O based phosphate buffered saline (PBS) solution, but ignorable amount was found in pure D_2O. Thus the IRRAS of adsorbed FN was measured at BML/D_2O interface. These experiments have been carried out allowing about 3 h for FN adsorption on BML surface after injection, and then FN in solution and loosely adsorbed FN were washed by flowing 2.50 ml pure D_2O through sample holder. The amide I band of FN was observed at approximately 1637 cm^{-1} (β sheet) with shoulders around 1671 and 1683 cm^{-1} (β turn). The component ratio of the secondary

structures was evaluated by deconvoluting the amide I band. The conformational change of FN due to the adsorption on the BML surface was not observed in this work.

The adsorbed FN on the BML surface at solid-solution interface was exposed to air, dried and observed by vacuum IRRAS. The amide I band of adsorbed FN appeared around 1664 cm^{-1} in vacuum, this indicated the denaturation of FN during the water removal from the substrate surface.

Protein adsorption on gold surface supplying good biocompability has been a major concern for the biochip application. I have investigated the adsorption state of immunoglobulin G (IgG) at the gold-solution interface with two differently modified gold surfaces i.e. 16-mercaptohexadecanoic acid (MHA)-SAM coated and activated MHA-SAM (N-(3-dimethylaminopropyl)-N'-ethylcarbodiimide hydrochloride (EDC) and N-hydroxysuccinimide (NHS) were used for MHA-SAM activation) coated gold surface. IgG was easily adsorbed on the PEG-coated prism surface in pure D_2O, but ignorable IgG was observed in the salt solution of D_2O such as NaCl (140 mM) added D_2O solution or D_2O based PBS solution or NaCl (140 mM) added D_2O based PBS solution. Therefore, NaCl (140 mM) added D_2O based PBS solution was chosen for the observation of IgG at gold-solution interfaces. IgG adsorption on the two modified gold surfaces were carried out by exposing the MHA-SAM modified gold surface and the activated MHA-SAM gold surface to the IgG solution for 1 h and 30 min, respectively. The excess IgG in solution was washed by 2.50 ml NaCl (140 mM) added D_2O based PBS solution.

Adsorbed IgG was measured by the NG-IRRAS on gold surfaces under D_2O-salt solution. The observed amide I band of IgG included the component at in the spectrum are 1639 cm^{-1} (β sheet), 1657 cm^{-1} (α helix), 1672 cm^{-1} (β turn), and 1683 cm^{-1} (β turn). On the activated MHA-SAM coated gold, IgG molecules are covalently bonded through the peptide bond. Absorption spectra of IgG in the solution and the covalently bonded IgG have been clearly observed in the IRRAS spectra with good reproducibility. I think that the molecular orientation of adsorbed IgG is random since lysine residues, which form covalent bond with –COOH on the MHA-SAM, are distributed almost

homogeneously on the IgG surface. Similarly, no clear adsorption-induced deformation was observed in the absorption spectrum of IgG adsorbed on the non-activated MHA-SAM coated gold surface.

Adsorbed IgG on these gold surfaces were measured by vacuum IRRAS arrangement. IgG also denatured, similar to FN due to the water removal from the gold surface and the wavenumber of amide I band moved to around 1666 cm^{-1}.

Although there is still admittance of improvement for suppressing the adsorption of proteins on CaF_2 prism surface, but this new NG-IRRAS can be especially applicable for observing antibody-antigen reaction on different non-transparent metal surface under solutions in physiological condition.

Appendix I

Spectrum processing and curve fitting

Spectrum processing

In this NG-IRRAS, a flat baseline was obtained using the proper flow rate and evacuation. But in some real experiments, some times distortion and water vapor noise were appeared in the spectra. Interference occurs in multilayer or solution system and their effects appear in the IR spectrum. Several mathematical processing techniques are used in previous works to remove these problems from the spectrum. These techniques are helpful to understand both the qualitative and quantitative interpretation of spectrum.

A slope correction procedure was applied to each spectrum to provide a horizontal baseline with zero values at 1760−1540 cm^{-1}. A data analyzing software Origin (Ver. 6, OriginLab Corp., MA) was used for the leveling of baseline and for removal of the interference from the spectrum. For removal of interference, FFT band block option was used with two values, such as low cut off and high cut off frequencies. These values were always chosen from the heights of the interference in the spectrum. In this works the values were around 0.04 and 0.07. To remove water vapor noise from the observed spectrum, a mathematical calculation was used.

$$f(\text{Water free observed spectrum}) = f(\text{observed spectrum}) \pm (k''/k') \times f(\text{standard water vapor spectrum})$$

The highest IR peak of the water vapor was found at 1652 cm^{-1} (H-O-H bending mode) in all observed spectra. The values of k' and k'' is measured from the observed and standard water vapor spectra. The standard spectrum of water vapor was obtained by calculating the spectra at 0.02 and 0.04 Torr. Depending upon the noise direction of the observed spectrum, addition or subtraction of the second term was carried out. Figure A1 for example shows the measured standard water vapor spectrum for this IRRAS system,

the value of the k' at 1652 cm^{-1} is about 0.00052; this value is used to minimize the vapor noise. If the noise was found in spectrum after removal of water vapor as well as interference, the spectrum was smoothed using the FFT smoothing option of the Origin program. After smoothing of a spectrum, it becomes similar to the result of an experiment at a lower resolution.

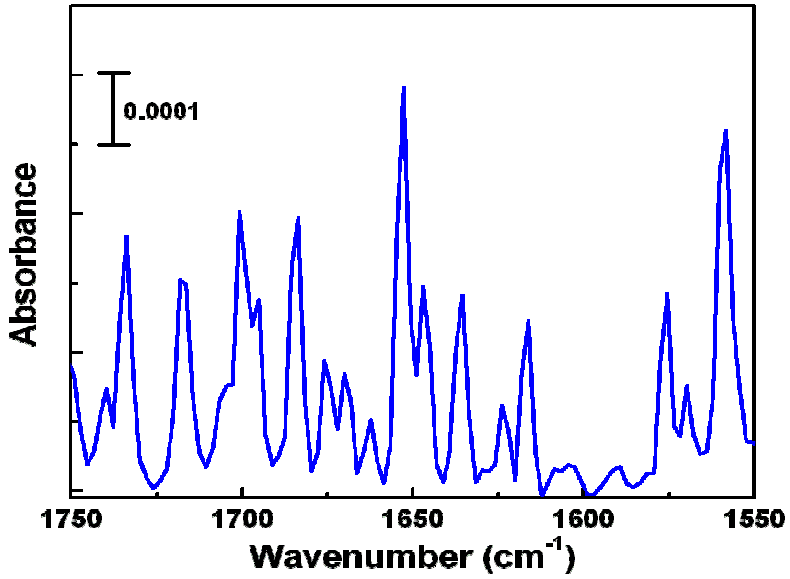

Figure A1 The standard water vapor spectrum for water noise minimization calculations.

Curve Fitting

In the spectrum of the amide I band, absorbance of different secondary structures such as α-helix, β-sheet, β-turns are overlapped. Accurate peak position of each secondary structure in amide I band can be obtained from the second derivative spectra, which was used for curve-fitting. In this work, non linear Gaussian curve fitting technique was chosen from the Origin program. For the curve fitting, initial peak positions and peak heights were presumed from the original data, and peak width was assumed to determine symmetric Gaussian curves. For the best fitting Gaussian curves, the spectrum positions and intensities of peaks were varied from the initial guesses and determined the best combination of the parameters. The component ratio of the secondary structures was evaluated from the integrated areas of the fitted Gaussians.

Appendix II

Refractive indexes of CaF_2 at different wavenumber

Wavenumber (cm^{-1})	Refractive index (n)
1110	1.32651
1135	1.32997
1160	1.33332
1190	1.33734
1220	1.34136
1250	1.34539
1265	1.34740
1280	1.34941
1300	1.35209
1315	1.35410
1335	1.35678
1350	1.35879
1370	1.36147
1390	1.36415
1410	1.36683
1430	1.36942
1450	1.37078
1470	1.37215
1490	1.37352
1515	1.37523
1540	1.37693
1560	1.3783
1590	1.38001
1610	1.38172
1640	1.38377
1665	1.38548
1695	1.38673

Refractive indexes of CaF_2 at different wavenumber

Wavenumber (cm^{-1})	Refractive index (n)
1725	1.38793
1755	1.38913
1785	1.39033
1820	1.39174
1850	1.39294
1885	1.39434
1925	1.39594
1960	1.39735
2000	1.39895
2040	1.39980
2085	1.40077
2130	1.40162
2175	1.40269
2220	1.40365
2270	1.40472
2325	1.40589
2380	1.40707
2440	1.40835
2500	1.40963
2565	1.41027
2630	1.41091
2700	1.41160
2775	1.41234
2875	1.41333
2900	1.41358
2940	1.41397
2985	1.41441

Appendix III

Extinction coefficient and Refractive indexes of water at different wavenumber

Wavenumber (cm^{-1})	Extinction coefficient (K)L/M-cm	Refractive index (n)
400	0.356	1.531
415	0.361	1.521
435	0.357	1.511
455	0.373	1.500
475	0.352	1.487
500	0.393	1.480
510	0.404	1.476
525	0.414	1.461
540	0.421	1.443
555	0.426	1.423
570	0.429	1.401
590	0.429	1.376
605	0.429	1.351
625	0.422	1.325
645	0.414	1.297
665	0.402	1.270
690	0.388	1.241
715	0.350	1.210
740	0.343	1.177
770	0.305	1.146
800	0.250	1.123
835	0.199	1.111
870	0.142	1.126
910	0.0968	1.152
950	0.0662	1.185
1000	0.0508	1.218
1020	0.0479	1.229
1040	0.0441	1.239
1065	0.0433	1.247
1085	0.0415	1.255
1110	0.0399	1.262
1135	0.0385	1.269
1160	0.472	1.276
1190	0.0361	1.281
1220	0.0351	1.286

Extinction coefficient and Refractive indexes of water at different wavenumber

Wavenumber (cm^{-1})	Extinction coefficient (K) L/M-cm	Refractive index (n)
1250	0.0343	1.291
1265	0.0339	1.294
1280	0.0335	1.297
1300	0.0331	1.299
1315	0.0328	1.302
1335	0.0326	1.304
1350	0.0324	1.307
1370	0.0322	1.309
1390	0.0321	1.312
1410	0.0320	1.314
1430	0.0320	1.317
1450	0.0322	1.321
1470	0.0327	1.324
1490	0.0337	1.329
1515	0.0356	1.334
1540	0.0392	1.339
1560	0.0449	1.347
1590	0.0370	1.357
1610	0.0880	1.363
1640	0.131	1.319
1665	0.107	1.265
1695	0.0622	1.248
1725	0.0330	1.262
1755	0.0203	1.277
1785	0.0142	1.289
1820	0.0116	1.293
1850	0.0100	1.306
1885	0.0098	1.312
1925	0.0101	1.317
1960	0.0111	1.322
2000	0.0124	1.325
2040	0.0137	1.328
2085	0.0150	1.330
2130	0.0157	1.330
2175	0.0447	1.330
2220	0.0434	1.332

Extinction coefficient and Refractive indexes of water at different wavenumber

Wavenumber (cm^{-1})	Extinction coefficient (K) L/M-cm	Refractive index (n)
2270	0.0403	1.334
2325	0.00845	1.338
2380	0.00688	1.342
2440	0.00562	1.346
2500	0.00460	1.351
2565	0.00380	1.357
2630	0.00340	1.364
2700	0.00336	1.374
2775	0.00616	1.385
2875	0.0094	1.400
2900	0.0132	1.410
2940	0.0195	1.420
2985	0.0261	1.432
3030	0.0368	1.450
3075	0.0610	1.467
3125	0.0921	1.78
3175	0.135	1.483
3225	0.192	1.467
3280	0.240	1.426
3330	0.272	1.371
3390	0.298	1.292
3450	0.268	1.201
3510	0.125	1.149
3570	0.115	1.142
3635	0.059	1.157
3705	0.019	1.185
3775	6.70×10^{-3}	1.219
3845	3.17×10^{-3}	1.242
4165	5.56×10^{-4}	1.279
4545	2.89×10^{-4}	1.296
5000	1.10×10^{-5}	1.306
5555	1.45×10^{-4}	1.342
6250	8.55×10^{-3}	1.317
7140	4.38×10^{-5}	1.321
8335	5.35×10^{-6}	1.324
10000	2.50×10^{-11}	1.327

Appendix IV

Thermal Expansion Co-efficient of Selected Materials

Materials	Thermal expansion coefficient (Θ) $\times(10^{-6}\ K^{-1})$
Aluminum	23.1
chromium	4.9
copper	16.5
germanium	6.1
glass	8.5
gold	14.2
Iron	11.8
Lead	28.9
Nickel	13.3
Platinum	8.8
Silicon	4.68
Silver	18.9
Tin	22
Titanium	4.5
zinc	30.2

Publication

1. **Md. Abu Sayed**, H. Uno, K. Harada, K. Tanaka, Y.-H. Kim, Y. Nakaoki, K. Okumura, R. Tero, T. Urisu, "New infrared reflection absorption spectroscopy (IRRAS) system for observation of solid-solution interface biomaterials" Chem. Phys. Lett. 466 (2008) 235.

International Conferences

1. **Md. A. Sayed**, H. Uno, Y.-H. Kim, R. Tero, T. Urisu, "New infrared reflection absorption spectroscopy system for in-situ observation of adsorbed biomaterials on solid surfaces under water" International Symposium on Surface Science and Nanotechnology *(ISSS-5*), International Conference Center, Waseda University, Tokyo, Japan, November, 2008

2. **Md. A. Sayed**, H. Uno, N. Misawa, R. Tero, T. Urisu, "New Infrared Reflection Absorption Spectroscopy System for in-situ Observation of Biomaterials under Water and in Vacuum", The Winter School of Sokendai/Asian CORE Program, National Institutes for Natural Sciences, Okazaki Conference Center, Japan, January, 2008

3. **Md. A. Sayed**, H. Uno, N. Misawa, R. Tero, K. Harada, K. Tanaka, T. Kondou, T. Urisu, "New In-situ Infrared Reflection Absorption Spectroscopy System for the Study of Biomaterials under Water", 1st International Symposium of Nanomedicine -from Basic to Applications- 2nd Molecule-Based Information Transmission and Reception (MB-ITR2007), Okazaki Conference Center, Japan, April, 2007

Conferences in Japan

1. **Md. A. Sayed**, H. Uno, Y.-H. Kim, R. Tero, T. Urisu, "Detection of Immunoglobulin G (IgG) on Gold Surface under Water and in Vacuum using a new In-situ Infrared Reflection Absorption Spectroscopic System" The 69th Autumn Meeting, The Japan Society of Applied Physics, Chubu University, Japan, September, 2008

2. **Md. A. Sayed**, H. Uno, N. Misawa, R. Tero, T. Urisu, "In-situ Infrared Reflection Absorption Spectroscopy System Using Buried Metal Layer Substrate (BML-IRRAS) for Biomaterials under Water", The 27th annual meeting of the Surface Science Society of Japan, University of Tokyo, Japan, November, 2007

3. **Md. A. Sayed**, H. Uno, N. Misawa, R. Tero, K. Harada, K. Tanaka, T. Kondou, K. Watanabe, T. Urisu, "Development of In-situ Infrared Reflection Absorption Spectroscopy System Using Buried Metal Layer Substrate (BML-IRRAS) for Biomaterials under Water", The 54th Spring Meeting, The Japan Society of Applied Physics and Related Societies, Aoyama Gakuin University, Kanazawa, Japan, March, 2007

4. **Md. A. Sayed**, H. Uno, N. Misawa, K. Harada, K. Tanaka, T. Kondou, R. Tero, T. Urisu, "In-situ Infrared Reflection Absorption Spectroscopy System Using Buried Metal Layer Substrate (BML-IRRAS) for Biomaterials under Water", The 67th Autumn Meeting, The Japan Society of Applied Physics, Ritsumeikan University, Japan, August, 2006

Acknowledgement

The research works in this thesis were carried out under the guidance of Prof. Urisu Tsuneo, Institute for Molecular Science (IMS). I am very grateful to him for his encouragement in the study and kindness in daily life. He has been very patient and kind to me when I had troubles in experiments and living life.

I would like to thank Dr. Ryugo Tero, research assistant of Prof. Urisu group, for his comments and advises on my thesis and help in my experiments. He has taught me many skills of scientific expression for my thesis and many experimental skills. I would like to thank Prof. Monimul Hoque and Prof. C. M. Mustafa for their occasional advises and comments on my work.

I would like to thank all the members of Urisu group, Toshifumi Asano, Hidetaka Uno, Naohito Nakai, Zhiguo Shang and Kynuo Fujiwara for their help and encouragement. It is my pleasure to do experiments in the same lab and join some activities with them together. I also would like to acknowledge the past members of this group, Dr. Mashiur Rahman, Dr. Nobuo Misawa, Dr. Yoon-Hoon Kim and Dr. Zenh-Long Zanh.

I sincerely thank Mr. Takuhiko Kondou and Mr. Mitsukazu Suzui, Institute for Molecular Science (IMS) for their technical supports.

I would like to thank Ms. Atsuko Shimizu, secretary of Urisu group, and Ms. Kyoko Kamo, secretary of the Foreign Affairs of IMS for their help in filling up some important documents on my studies and living in Okazaki.

I would like to extend my thanks to Prodhan Sirazul, Masud Reza, Ferdaous Nawoz, Habib, and other friends who inspired me to learn science. Finally, I would like to give my thanks to my parents, brother, sister and brother-in-law for their silent contributions. They are the source of happiness, motivation, and drive to achieve something worthwhile in life.